arXiv:hep-ex/9709003v1 5 Sep 1997

Search for the Standard Model Higgs Boson in e^+e^- Collisions at $\sqrt{s} = 161$ - 172 GeV .

The OPAL Collaboration

Abstract

This paper describes a search for the Standard Model Higgs boson using data from e^+e^- collisions collected at center-of-mass energies of 161, 170 and 172 GeV by the OPAL detector at LEP. The data collected at these energies correspond to integrated luminosities of 10.0, 1.0 and 9.4 pb^{-1}, respectively. The search is sensitive to the main final states from the process in which the Higgs boson is produced in association with a fermion anti-fermion pair, namely four jets, two jets with missing energy, and two jets produced together with a pair of electron, muon or tau leptons. One candidate event is observed, in agreement with the Standard Model background expectation. In combination with previous OPAL searches at center-of-mass energies close to the Z^0 resonance and the revised previous OPAL searches at 161 GeV , we derive a lower limit of 69.4 GeV for the mass of the Standard Model Higgs boson at the 95% confidence level.

(Submitted to Zeit. Phys. C)

The OPAL Collaboration

K. Ackerstaff[8], G. Alexander[23], J. Allison[16], N. Altekamp[5], K.J. Anderson[9], S. Anderson[12],
S. Arcelli[2], S. Asai[24], D. Axen[29], G. Azuelos[18,a], A.H. Ball[17], E. Barberio[8], R.J. Barlow[16],
R. Bartoldus[3], J.R. Batley[5], S. Baumann[3], J. Bechtluft[14], C. Beeston[16], T. Behnke[8], A.N. Bell[1],
K.W. Bell[20], G. Bella[23], S. Bentvelsen[8], S. Bethke[14], O. Biebel[14], A. Biguzzi[5], S.D. Bird[16],
V. Blobel[27], I.J. Bloodworth[1], J.E. Bloomer[1], M. Bobinski[10], P. Bock[11], D. Bonacorsi[2],
M. Boutemeur[34], B.T. Bouwens[12], S. Braibant[12], L. Brigliadori[2], R.M. Brown[20],
H.J. Burckhart[8], C. Burgard[8], R. Bürgin[10], P. Capiluppi[2], R.K. Carnegie[6], A.A. Carter[13],
J.R. Carter[5], C.Y. Chang[17], D.G. Charlton[1,b], D. Chrisman[4], P.E.L. Clarke[15], I. Cohen[23],
J.E. Conboy[15], O.C. Cooke[8], M. Cuffiani[2], S. Dado[22], C. Dallapiccola[17], G.M. Dallavalle[2],
R. Davis[30], S. De Jong[12], L.A. del Pozo[4], K. Desch[3], B. Dienes[33,d], M.S. Dixit[7], E. do Couto e
Silva[12], M. Doucet[18], E. Duchovni[26], G. Duckeck[34], I.P. Duerdoth[16], D. Eatough[16],
J.E.G. Edwards[16], P.G. Estabrooks[6], H.G. Evans[9], M. Evans[13], F. Fabbri[2], M. Fanti[2],
A.A. Faust[30], F. Fiedler[27], M. Fierro[2], H.M. Fischer[3], I. Fleck[8], R. Folman[26], D.G. Fong[17],
M. Foucher[17], A. Fürtjes[8], D.I. Futyan[16], P. Gagnon[7], J.W. Gary[4], J. Gascon[18],
S.M. Gascon-Shotkin[17], N.I. Geddes[20], C. Geich-Gimbel[3], T. Geralis[20], G. Giacomelli[2],
P. Giacomelli[4], R. Giacomelli[2], V. Gibson[5], W.R. Gibson[13], D.M. Gingrich[30,a], D. Glenzinski[9],
J. Goldberg[22], M.J. Goodrick[5], W. Gorn[4], C. Grandi[2], E. Gross[26], J. Grunhaus[23], M. Gruwé[8],
C. Hajdu[32], G.G. Hanson[12], M. Hansroul[8], M. Hapke[13], C.K. Hargrove[7], P.A. Hart[9],
C. Hartmann[3], M. Hauschild[8], C.M. Hawkes[5], R. Hawkings[27], R.J. Hemingway[6], M. Herndon[17],
G. Herten[10], R.D. Heuer[8], M.D. Hildreth[8], J.C. Hill[5], S.J. Hillier[1], P.R. Hobson[25], R.J. Homer[1],
A.K. Honma[28,a], D. Horváth[32,c], K.R. Hossain[30], R. Howard[29], P. Hüntemeyer[27],
D.E. Hutchcroft[5], P. Igo-Kemenes[11], D.C. Imrie[25], M.R. Ingram[16], K. Ishii[24], A. Jawahery[17],
P.W. Jeffreys[20], H. Jeremie[18], M. Jimack[1], A. Joly[18], C.R. Jones[5], G. Jones[16], M. Jones[6],
U. Jost[11], P. Jovanovic[1], T.R. Junk[8], D. Karlen[6], V. Kartvelishvili[16], K. Kawagoe[24],
T. Kawamoto[24], P.I. Kayal[30], R.K. Keeler[28], R.G. Kellogg[17], B.W. Kennedy[20], J. Kirk[29],
A. Klier[26], S. Kluth[8], T. Kobayashi[24], M. Kobel[10], D.S. Koetke[6], T.P. Kokott[3], M. Kolrep[10],
S. Komamiya[24], T. Kress[11], P. Krieger[6], J. von Krogh[11], P. Kyberd[13], G.D. Lafferty[16],
R. Lahmann[17], W.P. Lai[19], D. Lanske[14], J. Lauber[15], S.R. Lautenschlager[31], J.G. Layter[4],
D. Lazic[22], A.M. Lee[31], E. Lefebvre[18], D. Lellouch[26], J. Letts[12], L. Levinson[26], S.L. Lloyd[13],
F.K. Loebinger[16], G.D. Long[28], M.J. Losty[7], J. Ludwig[10], A. Macchiolo[2], A. Macpherson[30],
M. Mannelli[8], S. Marcellini[2], C. Markus[3], A.J. Martin[13], J.P. Martin[18], G. Martinez[17],
T. Mashimo[24], P. Mättig[3], W.J. McDonald[30], J. McKenna[29], E.A. Mckigney[15], T.J. McMahon[1],
R.A. McPherson[8], F. Meijers[8], S. Menke[3], F.S. Merritt[9], H. Mes[7], J. Meyer[27], A. Michelini[2],
G. Mikenberg[26], D.J. Miller[15], A. Mincer[22,e], R. Mir[26], W. Mohr[10], A. Montanari[2], T. Mori[24],
M. Morii[24], U. Müller[3], S. Mihara[24], K. Nagai[26], I. Nakamura[24], H.A. Neal[8], B. Nellen[3],
R. Nisius[8], S.W. O'Neale[1], F.G. Oakham[7], F. Odorici[2], H.O. Ogren[12], A. Oh[27],
N.J. Oldershaw[16], M.J. Oreglia[9], S. Orito[24], J. Pálinkás[33,d], G. Pásztor[32], J.R. Pater[16],
G.N. Patrick[20], J. Patt[10], M.J. Pearce[1], R. Perez-Ochoa[8], S. Petzold[27], P. Pfeifenschneider[14],
J.E. Pilcher[9], J. Pinfold[30], D.E. Plane[8], P. Poffenberger[28], B. Poli[2], A. Posthaus[3], D.L. Rees[1],
D. Rigby[1], S. Robertson[28], S.A. Robins[22], N. Rodning[30], J.M. Roney[28], A. Rooke[15], E. Ros[8],
A.M. Rossi[2], P. Routenburg[30], Y. Rozen[22], K. Runge[10], O. Runolfsson[8], U. Ruppel[14],

D.R. Rust[12], R. Rylko[25], K. Sachs[10], T. Saeki[24], E.K.G. Sarkisyan[23], C. Sbarra[29], A.D. Schaile[34], O. Schaile[34], F. Scharf[3], P. Scharff-Hansen[8], P. Schenk[34], J. Schieck[11], P. Schleper[11], B. Schmitt[8], S. Schmitt[11], A. Schöning[8], M. Schröder[8], H.C. Schultz-Coulon[10], M. Schumacher[3], C. Schwick[8], W.G. Scott[20], T.G. Shears[16], B.C. Shen[4], C.H. Shepherd-Themistocleous[8], P. Sherwood[15], G.P. Siroli[2], A. Sittler[27], A. Skillman[15], A. Skuja[17], A.M. Smith[8], G.A. Snow[17], R. Sobie[28], S. Söldner-Rembold[10], R.W. Springer[30], M. Sproston[20], K. Stephens[16], J. Steuerer[27], B. Stockhausen[3], K. Stoll[10], D. Strom[19], P. Szymanski[20], R. Tafirout[18], S.D. Talbot[1], S. Tanaka[24], P. Taras[18], S. Tarem[22], R. Teuscher[8], M. Thiergen[10], M.A. Thomson[8], E. von Törne[3], S. Towers[6], I. Trigger[18], Z. Trócsányi[33], E. Tsur[23], A.S. Turcot[9], M.F. Turner-Watson[8], P. Utzat[11], R. Van Kooten[12], M. Verzocchi[10], P. Vikas[18], E.H. Vokurka[16], H. Voss[3], F. Wäckerle[10], A. Wagner[27], C.P. Ward[5], D.R. Ward[5], P.M. Watkins[1], A.T. Watson[1], N.K. Watson[1], P.S. Wells[8], N. Wermes[3], J.S. White[28], B. Wilkens[10], G.W. Wilson[27], J.A. Wilson[1], G. Wolf[26], T.R. Wyatt[16], S. Yamashita[24], G. Yekutieli[26], V. Zacek[18], D. Zer-Zion[8]

[1]School of Physics and Space Research, University of Birmingham, Birmingham B15 2TT, UK
[2]Dipartimento di Fisica dell' Università di Bologna and INFN, I-40126 Bologna, Italy
[3]Physikalisches Institut, Universität Bonn, D-53115 Bonn, Germany
[4]Department of Physics, University of California, Riverside CA 92521, USA
[5]Cavendish Laboratory, Cambridge CB3 0HE, UK
[6] Ottawa-Carleton Institute for Physics, Department of Physics, Carleton University, Ottawa, Ontario K1S 5B6, Canada
[7]Centre for Research in Particle Physics, Carleton University, Ottawa, Ontario K1S 5B6, Canada
[8]CERN, European Organisation for Particle Physics, CH-1211 Geneva 23, Switzerland
[9]Enrico Fermi Institute and Department of Physics, University of Chicago, Chicago IL 60637, USA
[10]Fakultät für Physik, Albert Ludwigs Universität, D-79104 Freiburg, Germany
[11]Physikalisches Institut, Universität Heidelberg, D-69120 Heidelberg, Germany
[12]Indiana University, Department of Physics, Swain Hall West 117, Bloomington IN 47405, USA
[13]Queen Mary and Westfield College, University of London, London E1 4NS, UK
[14]Technische Hochschule Aachen, III Physikalisches Institut, Sommerfeldstrasse 26-28, D-52056 Aachen, Germany
[15]University College London, London WC1E 6BT, UK
[16]Department of Physics, Schuster Laboratory, The University, Manchester M13 9PL, UK
[17]Department of Physics, University of Maryland, College Park, MD 20742, USA
[18]Laboratoire de Physique Nucléaire, Université de Montréal, Montréal, Quebec H3C 3J7, Canada
[19]University of Oregon, Department of Physics, Eugene OR 97403, USA
[20]Rutherford Appleton Laboratory, Chilton, Didcot, Oxfordshire OX11 0QX, UK
[22]Department of Physics, Technion-Israel Institute of Technology, Haifa 32000, Israel
[23]Department of Physics and Astronomy, Tel Aviv University, Tel Aviv 69978, Israel
[24]International Centre for Elementary Particle Physics and Department of Physics, University

of Tokyo, Tokyo 113, and Kobe University, Kobe 657, Japan

[25]Brunel University, Uxbridge, Middlesex UB8 3PH, UK

[26]Particle Physics Department, Weizmann Institute of Science, Rehovot 76100, Israel

[27]Universität Hamburg/DESY, II Institut für Experimental Physik, Notkestrasse 85, D-22607 Hamburg, Germany

[28]University of Victoria, Department of Physics, P O Box 3055, Victoria BC V8W 3P6, Canada

[29]University of British Columbia, Department of Physics, Vancouver BC V6T 1Z1, Canada

[30]University of Alberta, Department of Physics, Edmonton AB T6G 2J1, Canada

[31]Duke University, Dept of Physics, Durham, NC 27708-0305, USA

[32]Research Institute for Particle and Nuclear Physics, H-1525 Budapest, P O Box 49, Hungary

[33]Institute of Nuclear Research, H-4001 Debrecen, P O Box 51, Hungary

[34]Ludwigs-Maximilians-Universität München, Sektion Physik, Am Coulombwall 1, D-85748 Garching, Germany

[a] and at TRIUMF, Vancouver, Canada V6T 2A3

[b] and Royal Society University Research Fellow

[c] and Institute of Nuclear Research, Debrecen, Hungary

[d] and Department of Experimental Physics, Lajos Kossuth University, Debrecen, Hungary

[e] and Department of Physics, New York University, NY 1003, USA

1 Introduction

Locally gauge-invariant theories of the electroweak interaction introduce spontaneous symmetry breaking to allow some of the gauge bosons to acquire mass while keeping the theory renormalizable. The Standard Model (SM) [1] is the simplest such theory and uses the self-interaction of a single doublet of complex scalar fields [2] to produce spontaneous symmetry breaking. This model predicts the existence of one physical scalar particle, the Higgs boson, H^0, whose couplings are fixed but whose mass is not predicted.

Despite a wide experimental effort, the Higgs boson has not yet been discovered. The experimental lower limits for its mass, m_{H^0}, obtained from large samples of Z^0 boson decays, are published in [3]. Recently the OPAL Collaboration has updated its result by including the data collected during summer 1996 at a center-of-mass energy of $\sqrt{s}$=161 GeV yielding a lower limit of 68.5 GeV on the Higgs boson mass [4]. During the autumn of 1996 the center-of-mass energy of the LEP e^+e^- collider was upgraded to 172 GeV.

At these center-of-mass energies, the main production process for the SM Higgs boson is $e^+e^-{\rightarrow}Z^0H^0$. The dominant decay is $H^0{\rightarrow}b\bar{b}$, with a branching ratio of approximately 86%. Other relevant decay modes are: $H^0{\rightarrow}\tau^+\tau^-$ (8%), $H^0{\rightarrow}c\bar{c}$ (4%), and $H^0{\rightarrow}$gluons (2%) [5]. For Higgs boson masses of current interest, these branching ratios exhibit only a mild dependence on the Higgs boson mass.

The searches described address the principal final state topologies, which account for about 95% of all Higgs boson final states, namely: (i) the four jets channel, $e^+e^-{\rightarrow}Z^0H^0{\rightarrow}q\bar{q}b\bar{b}$; (ii) the missing energy channel, mainly from $e^+e^-{\rightarrow}Z^0H^0{\rightarrow}\nu\bar{\nu}b\bar{b}$, with a small contribution from the W^+W^- fusion process $e^+e^-{\rightarrow}\nu\bar{\nu}H^0$; (iii) the tau channels, $e^+e^-{\rightarrow}Z^0H^0{\rightarrow}\tau^+\tau^-q\bar{q}$ and $q\bar{q}\tau^+\tau^-$; (iv) the muon and electron channels, predominantly from $e^+e^-{\rightarrow}Z^0H^0{\rightarrow}\mu^+\mu^-q\bar{q}$ and $e^+e^-q\bar{q}$, with the latter including a small contribution from the Z^0Z^0 fusion process $e^+e^-{\rightarrow}e^+e^-H^0$.

The present paper describes the analysis of the data collected at 170 and 172 GeV energies, an improved analysis of the four jets channel for the 161 GeV data based on likelihood rather than cut-based methods, and the derivation of a new mass limit.

2 Detector, Data, and Simulations

This analysis uses 1.0 pb^{-1} of data recorded with the OPAL detector [6] at $\sqrt{s}$=170 GeV, 9.4 pb^{-1} at $\sqrt{s}$=172 GeV and 10.0 pb^{-1} at $\sqrt{s}$=161 GeV for the four jets channel.

OPAL is a multipurpose apparatus with nearly complete solid angle coverage and excellent hermeticity. The central tracking detector consists of two layers of silicon microstrip detectors [7] with polar angle[1] coverage $|\cos\theta| < 0.9$, immediately outside the beam-pipe, followed by a high-precision vertex drift chamber, a large-volume jet chamber, and z-chambers, all in a

---

[1]OPAL uses a right-handed coordinate system where the $+z$ direction is along the electron beam and where

uniform 0.435 T axial magnetic field. A lead-glass electromagnetic calorimeter is located outside the magnet coil, which, in combination with the forward calorimeter, gamma catcher, and silicon-tungsten luminometer [8], provide acceptance down to 24 mrad from the beam direction. The silicon-tungsten luminometer serves to measure the integrated luminosity using small-angle Bhabha scattering events [9]. The magnet return yoke is instrumented with streamer tubes for hadron calorimetry and is surrounded by several layers of muon chambers. Events are reconstructed from charged-particle tracks and energy deposits ("clusters") in the electromagnetic and hadronic calorimeters. The tracks and clusters are required to pass a set of quality requirements similar to those used in previous Higgs boson searches [10]. In calculating the total visible energy and momentum, E_{vis} and $\vec{P}_{\mathrm{vis}}$, of events and of individual jets, corrections are applied that reduce the effect of double-counting of energy in the case of tracks and clusters associated to them.

The signal detection efficiencies and accepted background cross sections are estimated using a variety of Monte Carlo samples all processed through a full simulation [11] of the OPAL detector. The HZHA generator [12], including initial-state radiation effects, is used to simulate Higgs boson production processes. The generated partons are hadronized using JETSET [14]. Signal samples are produced for fixed values of $m_{\mathrm{H^0}}$ between 40 GeV and 80 GeV. The estimates of the different background processes are based primarily on the following event generators: PYTHIA [14] ($\mathrm{Z^0}/\gamma^* \to q\bar{q}(\gamma)$), grc4f [15] (four-fermion processes including $\mathrm{W^+W^-}$ and $\mathrm{Z^0Z^*}$), BHWIDE [16] ($\mathrm{e^+e^-}(\gamma)$), KORALZ [17] ($\mu^+\mu^-(\gamma)$ and $\tau^+\tau^-(\gamma)$), PYTHIA, PHOJET [18] and Vermaseren [19] (hadronic and leptonic two-photon processes).

3   The Four Jets Channel

The process $\mathrm{e^+e^-} \to \mathrm{Z^0H^0} \to q\bar{q}b\bar{b}$ amounts to approximately 60% of the Higgs boson signal topologies. It is characterized by four energetic hadronic jets, large visible energy and signals from b-hadron decays. The backgrounds are $\mathrm{Z^0}/\gamma^* \to q\bar{q}$ with and without initial state radiation accompanied by hard gluon emission as well as four-fermion processes, in particular $\mathrm{e^+e^-} \to \mathrm{W^+W^-}$. The suppression of these backgrounds relies on the kinematic reconstruction of the $\mathrm{Z^0}$ boson and on the identification of b-quarks from the Higgs boson decay. The tagging of particles containing b quarks proceeds by detecting displaced secondary vertices in three dimensions exploiting the high-resolution obtained from OPAL's silicon microvertex detector and using leptons with high transverse momenta with respect to the jets to which they are assigned.

The selection of candidate events and the suppression of background is done in two steps. A preselection using cuts is first performed in order to retain only events which have some similarity to the signal. The remaining events are then analyzed using a likelihood technique.

This channel was already analyzed and published using cut-based methods for the 161 GeV

$+x$ points to the center of the LEP ring. The polar angle, θ, is defined with respect to the $+z$ direction and the azimuthal angle, ϕ, with respect to the horizontal, $+x$ direction.

data [4], however, using likelihood methods and a better b-tag improves the signal efficiency significantly with the same expected background. The analysis of this channel was therefore repeated for the 161 GeV data with the new likelihood method.

The analysis proceeds in the following way:

First, large parts of the $Z^0/\gamma^* \to q\bar{q}$ background are eliminated by selecting well defined four jet topologies using the cuts listed below:

(1) The events must qualify as a hadronic final state according to ref. [20].

(2) The radiative process $e^+e^- \to Z^0\gamma \to q\bar{q}\gamma$ is largely eliminated by requiring that the effective center-of-mass energy, $\sqrt{s'}$, obtained by discarding the radiative photon from the event [21], is at least 140 GeV (150 GeV) at $\sqrt{s} = 161$ GeV ($\sqrt{s} = 170 - 172$ GeV).

(3) The final state particles of an event are grouped into four jets using the Durham algorithm [22]. The jet resolution parameter, y_{34}, at which the number of jets changes from 3 to 4, is required to be larger than 0.005.

(4) The $Z^0/\gamma^* \to q\bar{q}$ background is further suppressed by requiring that the event shape parameter C [23], which is large for spherical events, is larger than 0.45.

(5) All four jets are required to contain at least two tracks and two electromagnetic calorimeter clusters.

(6) To discriminate against poorly reconstructed events, a kinematic fit, using energy and momentum conservation constraints (4C-fit), is required to converge with a probability larger than 0.01.

The $e^+e^- \to H^0Z^0$ hypothesis is tested by a kinematic fit which, in addition to the energy and momentum conservation constraints, also forces two of the four jets to have an invariant mass equal to the Z^0 boson mass (5C-fit). This fit is applied in turn to all six possible associations of the four jets to the Z^0 and H^0 bosons. The fit is required to converge for at least one combination with a probability of at least 0.01. The combination yielding the highest χ^2-probability is selected.

Table 1 shows the number of events selected in data and Monte Carlo at each stage of the cuts for both center-of-mass energies. After removing most of the two-photon background (cut(1)), a good agreement between the observed data and the expected background can be seen.

Next, a likelihood technique is employed in order to classify the remaining events as either $Z^0/\gamma^* \to q\bar{q}$ (1), a four-fermion process (2) or $Z^0H^0 \to q\bar{q}b\bar{b}$ (3). To select signal events with low background, the information from 14 quantities (described below) which provide a good separation between the three different event classes is combined. Half of the variables are related to the kinematics of the events, and the other half are related to b-tagging. For each event the measured values x_i (i=1...14) of these variables are compared with probability density

6

Cut	Data 161 GeV	Total bkg.	$q\bar{q}(\gamma)$	4-ferm.	Efficiency (%) $m_{\mathrm{H^0}} = 65$ GeV
(1)	1572	1389.4	1345.9	52	99.9
(2)	395	377.5	351.1	26.4	89.5
(3)	65	54.1	38.0	16.1	81.4
(4)	51	40.6	26.2	14.4	75.6
(5)	49	33.2	21.5	11.7	70.5
(6)	26	24.2	14.0	10.2	62.3
$\mathcal{L}^{HZ} > 0.9$	0	0.75 ± 0.08	0.49	0.26	32.1

Cut	Data 170-172 GeV	Total bkg.	$q\bar{q}(\gamma)$	4-ferm.	Efficiency (%) $m_{\mathrm{H^0}} = 68$ GeV
(1)	1409	1306.7	1189.7	117.0	99.7
(2)	367	381.2	312.8	68.4	87.8
(3)	93	84.7	33.5	51.2	79.3
(4)	77	70.9	22.9	48.0	75.8
(5)	68	60.3	18.1	42.2	70.2
(6)	56	50.3	12.6	37.7	61.4
$\mathcal{L}^{HZ} > 0.925$	1	0.88 ± 0.07	0.34	0.55	28.4

Table 1: *The number of events after each cut of the selection for the data at $\sqrt{s} = 161$ (170-172) GeV and the expected background in the four jets channel. The background estimates are normalized to 10.0 (10.4 pb^{-1}). The last column shows the selection efficiencies for the $\mathrm{Z^0 H^0 \rightarrow q\bar{q}b\bar{b}}$ final state.*

functions normalized to unity obtained from Monte Carlo events processed through the full detector simulation. The likelihood for each event to belong to any of the three event classes is calculated as follows. For a single variable, the probability for an event to belong to class j is given by

$$p_i^j(x_i) = \frac{f_i^j(x_i)}{\sum_{k=1}^3 f_i^k(x_i)},$$

where $f_i^j(x_i)$ denotes the probability density for event class j and variable i. The likelihood function for class j is defined as the normalized product of the $p_i^j(x_i)$

$$\mathcal{L}^j(\vec{x}) = \frac{\prod_{i=1}^n p_i^j(x_i)}{\sum_{k=1}^3 \prod_{i=1}^n p_i^k(x_i)},$$

where $n = 14$ is the number of variables. In order to select an event as a candidate event its likelihood for being a signal event is required to be larger than a certain value depending on the preferred signal/background ratio.

The first set of variables entering the likelihood function exploit the different kinematics of the background and signal events: the smallest angle between any pair of jets (1), the smallest dijet mass (2), the highest and lowest jet energy (3-4) and the dijet mass closest to m_{Z^0} (5). All these quantities are calculated after the 4C-fit. The probability of the best kinematic fit requiring energy and momentum conservation and equal dijet masses (6) and the larger $\beta = p/E$ factor of the two dijet momenta calculated from the jet pair combination closest to the WW hypothesis (7) are also used. The best jet pair combination under the WW hypothesis is determined by minimizing $(p_{\mathrm{dijet1}} - x)^2 + (p_{\mathrm{dijet2}} - x)^2$, where x is 30 GeV at 170-172 GeV and 6 GeV at 161 GeV center of mass energy. This quantity vanishes for perfectly reconstructed on-shell WW events.

The second set of variables is used to tag b-flavored hadrons. Secondary vertices are identified in each jet separately using the three dimensional extension of the method described in [24]. To improve the quality of the vertices, each accepted vertex is required to have at least two tracks containing 2 silicon microvertex hits in both $r\phi$ and z. The variables to discriminate between b flavor and lighter flavors are: sum of the decay length significances of the vertices found in the candidate Higgs jets (8)[2], the maximum number of tracks with significantly large impact parameter (9)[3], the invariant mass of the tracks in the vertex with the largest decay length significance (10), the smaller of the two Higgs jet masses (11), the sum of the momenta of the highest momentum track associated with each vertex of the two Higgs jets (12), the largest transverse momentum of an identified lepton (electron or muon) with respect to the corresponding jet axis (13) and the sum of the two largest numbers of significant tracks in the four jets (14).

Finally the likelihood for each event is required to be larger than 0.90 at $\sqrt{s} = 161$ GeV and larger than 0.925 at $\sqrt{s} = 170 - 172$ GeV (i.e. $\mathcal{L}^3(\vec{x}) > 0.90$ (0.925)). The likelihood

---

[2]The decay length significance is defined as L/σ_L, where L is the three dimensional distance between the primary and the secondary vertex and σ_L is the corresponding error.

[3]Significant tracks are defined by $d/\sigma_d > 2.5$ where d denotes the two dimensional impact parameter of the track and σ_d the error on the impact parameter.

requirement was tightened for the higher center of mass energy in order to retain the same level of expected background for both energies.

The analysis was tuned with a reference mass of $m_{H^0} = 65$ GeV (68 GeV) at $\sqrt{s}= 161$ GeV (170-172 GeV) with a resulting efficiency of 32.1% (28.5%). The resulting expected background is 0.49 (0.34) events from Z/γ^* and 0.26 (0.55) events from 4-fermion processes. Other sources of background are negligible. The total expected background is 0.75±0.08(stat)±0.25(syst) (0.88±0.07±0.18) events. The background systematics are dominated by the error on the modeling of the variables used in the likelihood.

For all fourteen input quantities a good agreement between OPAL data and the Monte Carlo (MC) distributions is observed. This can be seen in Figure 1 where some distributions of data and simulated background as well as a simulated 68 GeV Higgs signal are shown. The agreement between MC and data, in particular for b-tag related quantities, was also checked at $\sqrt{s}=m_{Z^0}$ with data taken for calibration immediately before the high energy runs.

Figures 2 (a) and (b) show the distributions of the signal likelihood for the preselected events from the 161 GeV and 170-172 GeV data. The shaded area shows the expectation from 4-fermion events, the white area is Z/γ^* events and the dotted line represents the total background with a signal from a 65 GeV Higgs at $\sqrt{s} = 161$ GeV and a 68 GeV Higgs at $\sqrt{s} = 170$-172 GeV added. It can be seen that the expected signal is concentrated at large values of the likelihood. The peak of the background at large likelihood values is due to irreducible signal like four-fermions and QCD four jets events containing b flavor.

No event survived the likelihood cut of 0.9 at $\sqrt{s} = 161$ GeV. With a cut at 0.925 in the likelihood variable one candidate event is selected from the data collected at $\sqrt{s} = 172$ GeV. The likelihood of this event is 0.993. The invariant mass of the two jets associated with the Higgs boson decay is 75.6±3.0 GeV. Both of the Higgs candidate jets have displaced secondary vertices with significances of 6.1 and 2.0, and charged multiplicities of 4 and 3. One of the jets assigned to the Z^0-candidate has also a displaced secondary vertex with a significance of 4.6 and multiplicity of 2. The event is shown in Figure 8.

The likelihood method has been also checked using calibration events at a LEP energy of $\sqrt{s} = m_{Z^0}$ where the physics is well established. Events classified as four jets are selected and the tracks momenta and clusters energies are scaled up to 172 GeV center of mass energy. The b-tag information and most of the kinematic event properties are preserved by the procedure. The likelihood values of the scaled events show a good agreement between data and MC simulation (see Figure 4).

The signal detection efficiencies at $\sqrt{s} = 161$ GeV (170-172 GeV) are affected by the following uncertainties: Monte Carlo statistical error 4% (2%); description of preselection variables 5% (2%); modeling of the variables used in the likelihood selection, 10% (7%). The latter was dominated by b-tag variables uncertainties which were estimated by varying the tracking resolution. The modeling was also checked using a re-weighting procedure. The difference between data and MC distributions was minimized by assigning weights to all MC events in an iterative procedure and recalculating the likelihood with the weighted MC distributions. The binning of

9

reference distributions yielded a contribution to the systematic error of 1% (2%). Taking these uncertainties as independent and adding them in quadrature results in a total systematic error on the signal efficiency of 12% (8%) relative error.

Two additional analyses were performed as a check of the likelihood method. The first was a cut-based method similar to the published analysis of the 161 GeV data [4]. This analysis gave, for similar residual background, signal efficiencies which were lower by 10-20% than those of the current analysis. Applied to the 170-172 GeV data, the cut-based analysis did not select the candidate event selected by the current selection because it failed the cut in the event shape parameter C. The C-parameter of this event is 0.546, close to the cut value of 0.55.

Another multidimensional analysis utilizing an Artificial Neural Network (ANN) with 9 b-quark tagging variables and 12 kinematic variables was also performed. Using the same Monte Carlo signal and background samples described previously, the ANN analysis achieved similar efficiency, signal-to-noise and systematic errors, to the likelihood approach. The ANN identified one Higgs boson candidate with a cut on the ANN output variable corresponding to a background of 0.9 events. This event was the same as the one identified in the main analysis.

4   The Missing Energy Channel

The $e^+e^- \rightarrow \nu\bar{\nu}H^0 \rightarrow \nu\bar{\nu}b\bar{b}$ process amounts to approximately 18% of the Higgs boson signal topologies with a small contribution (0.7% for $m_{H^0}=68$ GeV) from the W^+W^- fusion process $e^+e^- \rightarrow \nu\bar{\nu}H^0 \rightarrow \nu\bar{\nu}b\bar{b}$. These events are characterized by large missing momentum and two energetic, acoplanar, hadronic jets containing b-hadrons. The dominant backgrounds are mismeasured $Z^0/\gamma^* \rightarrow q\bar{q}$ events, four-fermion processes with neutrinos in the final state, such as $W^+W^- \rightarrow \ell^\pm\nu q\bar{q}$ and $W^\pm e^\mp\nu \rightarrow q\bar{q}\,e^\mp\nu$ with the charged lepton escaping detection and, in general, events in which particles go undetected down the beam pipe such as $e^+e^- \rightarrow Z^0\gamma$ and two-photon events. For most of these backgrounds, the missing momentum vector points close to the beam direction, while signal events tend to have missing momentum in the transverse plane.

The event selection proceeds as follows:

(1) To reduce two-photon and beam-wall interactions, the number of tracks passing the quality cuts [10] should be greater than six, and should exceed 20% of the total number of tracks in the event. The energy deposited in the forward detector, gamma catcher and silicon-tungsten luminometer must be less than 2 GeV, 5 GeV, and 5 GeV, respectively. The fraction of energy deposited in the region $|\cos\theta| > 0.9$ must not exceed 50% of the total visible energy in the event. The total transverse momentum of the event, $P_{\rm vis}^T$, must be greater than 1 GeV and the visible mass must satisfy $m_{\rm vis} > 4$ GeV.

(2) To remove backgrounds in which particles go undetected down the beam pipe, the polar angle, $\theta_{\rm miss}$, of the missing momentum ($\vec{P}_{\rm miss} = -\vec{P}_{\rm vis}$) must satisfy $|\cos\theta_{\rm miss}| < 0.9$. The

z component of the visible momentum, P_{vis}^z, is required to be less than 30 GeV.

(3) The remaining two-photon background is eliminated by requiring $P_{\text{vis}}^T > 8$ GeV. As a precaution against large fluctuations in the measured hadronic energy, P_{vis}^T is recalculated excluding hadronic calorimeter clusters and is also required to be larger than 8 GeV.

(4) The remaining events are reconstructed as two-jet events using the Durham algorithm. The axes of both jets are required to have a polar angle satisfying $|\cos\theta| < 0.9$, to ensure good containment.

(5) The remaining background from $Z^0/\gamma^* \to q\bar{q}$ is characterized by two jets that tend to be back-to-back with small acoplanarity angles (where the acoplanarity angle is defined as $180° - \phi_{jj}$ where ϕ_{jj} is the angle between the two jets in the plane perpendicular to the beam axis), in contrast to signal events in which the jets are expected to have some acoplanarity angle due to the boost of the Higgs boson. This background is suppressed by requiring that the jet-jet acoplanarity angle be larger than $5°$.

(6) Since the Higgs boson recoils against a Z^0 boson decaying into a pair of neutrinos, the signal has a missing mass close to m_{Z^0}. The remaining backgrounds, predominantly from well contained multi-hadron and four-fermion events including semi-leptonic W^+W^- decays, typically have small missing masses. These backgrounds are reduced by the missing mass requirement $76^2 < m_{\text{miss}}^2 < 120^2$ GeV^2. The distribution of the missing mass squared after cut (5) is shown in Figure 5.

(7) W^+W^- events with one of the W bosons decaying leptonically and the other decaying into hadronic jets are rejected by requiring that the events have no isolated leptons.

In this context, leptons are low-multiplicity jets with one (two or three) tracks associated to electromagnetic or hadronic energy clusters, confined to a cone of $5°$ ($7°$) half-angle, having an invariant mass less than 2.5 GeV and momentum in excess of 5 GeV. The lepton is considered isolated if the sum of the track energy and the electromagnetic energy contained between the above lepton cone and an isolation cone of $25°$ half-angle does not exceed 10% (15%) of the lepton energy. If the lepton cone has only one track, the isolation cone is not allowed to contain another track.

(8) The remaining background is mostly from semi-leptonic W^+W^- and $We\nu$ events where the charged lepton goes undetected down the beam pipe. These events are suppressed by requiring b-hadrons in the hadronic jets of events with a visible mass close to the W boson mass. Each of the two hadronic jets is required to contain a secondary vertex with at least two tracks, each containing two silicon microvertex detector $r\phi$ hits. The two vertices are reconstructed according to the three dimensional extension of the method used in [24]. The correlation between the sum of the decay length significances, Σ_S, and the visible mass of the event is shown in Figure 6 where the two-dimensional cut employed is also shown.

The numbers of observed and expected events after each selection cut are given in Table 2, along with the detection efficiency for a 68 GeV Higgs boson. No events survive the cuts while

11

the expected background is of 0.55±0.05(stat)±0.10(syst) events. The background systematics is dominated by the error on the modelling of the cut variables.

One event is rejected only by the b-tag requirement. This event has two well-contained hadronic jets and evidence for an isolated muon pointing at the very forward direction where no tracking information is available. The muon appears as electromagnetic and hadronic clusters aligned with two muon chambers hits. With a well-measured muon, this event would be classified as $W^+W^- \rightarrow q\bar{q}\mu\nu$ and rejected by the isolated leptons veto.

The detection efficiencies as a function of the Higgs boson mass are listed in Table 5. These include a small correction (2.3%) due to accelerator-related backgrounds in the forward detectors which are not simulated. The detection efficiencies are affected by the following uncertainties: Monte Carlo statistics, 2.2%; modeling of the cut variables other than b-tagging, 3.8%; b-tagging and uncertainties from fragmentation and hadronization 3.0% and lepton tag, 5.6%. Taking these uncertainties as independent and adding them in quadrature results in a total relative systematic uncertainty of 7.7%.

Cut	Data	Total bkg.	$q\bar{q}(\gamma)$	4-ferm.	$\gamma\gamma$	Efficiency (%) m_{H^0} = 68 GeV
(1)	2984	2829	713	105	2011	83.3
(2)	1468	1486	302.1	86.7	1097	73.6
(3)	173	177.5	121.0	56.0	0.37	71.9
(4)	163	165.9	113.5	52.0	0.30	64.3
(5)	53	58.5	18.3	40.0	0.30	62.3
(6)	2	2.2	0.6	1.5	0.1	55.2
(7)	1	1.6	0.52	1.0	0.1	52.8
(8)	0	0.55±0.05	0.275	0.275	0	42.7

Table 2: *The numbers of events after each cut for the data and the expected background for the missing energy channel. The background estimates are normalized to* 10.4 pb^{-1}. *The quoted error is statistical. The last column shows the selection efficiencies for the* $\nu\bar{\nu}(H^0 \rightarrow$ all) *final state, for a 68* GeV *Higgs boson.*

5   The Tau Channels

The $\tau^+\tau^- q\bar{q}$ final state can be produced via the processes $e^+e^- \rightarrow Z^0 H^0 \rightarrow \tau^+\tau^- q\bar{q}$ (about 3% of the total $Z^0 H^0$ production rate) and $q\bar{q}\tau^+\tau^-$(about 5.6%). This analysis is sensitive to both processes, which are characterized by a pair of tau leptons and a pair of energetic hadronic jets. In addition, either the pair of hadronic jets or the pair of tau leptons should have an invariant mass consistent with the Z^0 mass. These characteristics are used to suppress the backgrounds, predominantly from $Z^0/\gamma^* \rightarrow q\bar{q}$ and four-fermion processes.

The selection begins with the identification of tau leptons using three algorithms which address the different decay channels of the tau lepton.

(a) An electron, identified by a neural network algorithm [25], is classified as a $\tau^{\pm} \to e^{\pm} \nu \bar{\nu}$ decay if its momentum is larger than 2 GeV, and it is isolated. In particular, the number of electromagnetic clusters within a cone of 26° half-angle around the electron track, N_{em}^{26}, must be less than six, and the ratio of the electromagnetic energy within an 11° cone to that within a 30° cone, $R_{em}^{11/30}$ must be greater than 0.7. There must be no hadronic calorimeter cluster with energy greater than 0.6 GeV that is associated with the electron track. Electrons from photon conversions are rejected using a neural network algorithm [26].

(b) A muon, identified using standard selection algorithms [27], is classified as a $\tau^{\pm} \to \mu^{\pm} \nu \bar{\nu}$ decay if its momentum is larger than 3 GeV, and if it is isolated. In particular, $N_{em}^{26} < 5$, and the ratio of the scalar sum of all track momenta within an 11° cone to that within a 30° cone, $R_{cd}^{11/30}$, must be greater than 0.7.

(c) The remaining tau lepton decays are identified as narrow, isolated jets. Jets are re-constructed using a cone algorithm [28] with a half-angle of 23° and with at least 3 GeV of associated energy. Within each resulting jet, the sub-jet of 11° half-angle having the highest energy is formed. The sub-jets are accepted as tau candidates if they satisfy the fiducial requirement $|\cos\theta| < 0.92$, have one or three associated tracks, have an invariant mass less than 3.5 GeV, and are isolated with $R_{em}^{11/30} > 0.6$.

In the selection that follows, the tau lepton momentum is approximated by the momentum of the visible decay products. When there are two tau lepton candidates with momentum vectors separated by less than 23°, one being identified as a leptonic decay (algorithms (a) or (b)) and one as a narrow jet (algorithm (c)), only the candidate identified as a leptonic decay is selected.

(1) Events are required to have at least two tau lepton candidates, each with charge of $|q| = 1$.

(2) The total track multiplicity of the event must exceed eight.

(3) Most of the two-photon and $e^+e^- \to Z^0\gamma$ background events are eliminated by requiring that the energy in the forward detector, gamma catcher, and silicon-tungsten luminometer be less than 4, 10, and 10 GeV, respectively, that $|\cos\theta_{miss}| < 0.97$ and that $P_{vis}^T > 3$ GeV. In addition, the scalar sum of all track and cluster transverse momenta is required to be larger than 40 GeV.

(4) The remaining $Z^0/\gamma^* \to q\bar{q}$ background, with and without photon radiation, is further suppressed by requiring that events contain at least four jets, reconstructed using the cone algorithm with a 23° half-angle as in (c) above (single electrons and muons from tau lepton decays are recognized as low-multiplicity "jets"). Events with an energetic isolated photon[4] are removed.

---

[4] An energetic isolated photon is defined in this context as an electromagnetic cluster with energy larger than 15 GeV and no track within a cone of 30° half-angle.

13

(5) In signal events, the algorithms (a), (b), and (c) identify 2.3 tau candidates per event on the average. Fake tau candidates containing 3 charged tracks are removed by requiring that the tracks originate from a common vertex in three dimensions, as reflected by a χ^2 probability of a vertex fit larger than 1%. Fake candidate pairs are further removed by requiring that the sum of the track charges be zero and that the tau candidates satisfy a pairwise isolation requirement, $|\cos\alpha_1 \cdot \cos\alpha_2| < 0.8$, where α_i is the angle between the direction of the ith tau candidate and that of the nearest track not associated with it. In those rare instances where more than one candidate pair passes the selection, we give preference to those pairs having taus which were identified through their leptonic decay mode and, in case of further ambiguity, we choose the pair with the lowest charged multiplicity and highest isolation.

The hadronic part of the event, obtained by excluding the tracks and clusters from the selected tau candidate pair, is then split into two jets using the Durham algorithm. The invariant masses of the tau lepton pair, $m_{\tau\tau}$, and of the hadron jets, m_{had}, are calculated using only the tau lepton and jet momentum directions and requiring energy and momentum conservation. At this point the selection separates into two parts, one (A) sensitive to the $(\mathrm{Z}^0{\to}\tau^+\tau^-)(\mathrm{H}^0{\to}\mathrm{q\bar{q}})$ process and another (B) sensitive to the $(\mathrm{Z}^0{\to}\mathrm{q\bar{q}})(\mathrm{H}^0{\to}\tau^+\tau^-)$ process.

(6) (6A) The selected events must satisfy 75 GeV $< m_{\tau\tau} <$ 105 GeV and $m_{\mathrm{had}} >$30 GeV. In addition, E_{vis} is required to be less than 155 GeV, since the neutrinos from the tau lepton decays, originating from the Z^0 boson, give rise to a relatively large missing energy. Finally, cuts are implemented to suppress specific four-fermion backgrounds, from $\mathrm{e}^+\mathrm{e}^-{\to}\mathrm{Z}^0/\gamma^* + \mathrm{Z}^0/\gamma^*$ and $\mathrm{e}^+\mathrm{e}^-{\to}\mathrm{Z}^0\mathrm{e}^+\mathrm{e}^-$. If the tau lepton candidates are both classified as $\tau^\pm{\to}\mathrm{e}^\pm\nu\bar{\nu}$ or both as $\tau^\pm{\to}\mu^\pm\nu\bar{\nu}$, their opening angle is required to be larger than $90°$ and, in the first case, neither electron is allowed to lie within $36°$ of the beam axis.

(6B) The selected events must satisfy 75 GeV $< m_{\mathrm{had}} <$ 105 GeV and $m_{\tau\tau} >$ 30 GeV. Since in this case the mass cuts are less effective against the background, the requirements on the properties of the tau lepton candidates are tightened. The opening angle of the tau lepton pair must be larger than $110°$ and, if one of the tau candidates has a track multiplicity exceeding two, the pairwise isolation cut is tightened to $|\cos\alpha_1 \cdot \cos\alpha_2| < 0.55$. Furthermore, to suppress four-fermion backgrounds, pairs with leptons of the same flavor are rejected. Finally, to suppress the process $\mathrm{W}^+\mathrm{W}^-{\to}\ell\nu\mathrm{q\bar{q}}$, events are rejected if they contain any track or cluster with a momentum or energy exceeding 40 GeV.

Distributions of $|\cos\alpha_1 \cdot \cos\alpha_2|$ and $m_{\tau\tau}$ are shown in Figures 7 and 8 for the data, the backgrounds, and for a 68 GeV Higgs boson signal, with $\mathrm{H}^0{\to}\tau^+\tau^-$. The numbers of observed and expected events after each stage of the selection are given in Table 3 where a good agreement between data and MC can be seen. The detection efficiency for a 68 GeV Higgs boson is also given. No candidate event is observed while the total background for selections A and B is estimated to be 0.59±0.04(stat)±0.14(syst) events. The background systematics is dominated by the error due to the modeling of the cut variables.

The detection efficiencies for cases A and B as a function of the Higgs boson mass are given in Table 5. and include a small correction coming from accelerator-related backgrounds in the forward detectors (2.3 %) which are not fully simulated. The detection efficiencies are affected by the following uncertainties: Monte Carlo statistics, 2.8%; uncertainty in the tau lepton identification efficiency, 4.3%; uncertainties in the modeling of cut variables excluding the tau lepton identification, 9.1% (case A) and 7.6% (case B); uncertainties in the modeling of fragmentation and hadronization, 1.2%. Taking these uncertainties as independent and adding them in quadrature results in a total systematic uncertainty of 10.5% (case A) and 9.2% (case B) (relative errors).

Cut	Data	Total bkg.	$q\bar{q}(\gamma)$	4-ferm.	$\gamma\gamma$	$\ell^+\ell^-$	$\epsilon(\%)$, case A 68 GeV	$\epsilon(\%)$, case B 68 GeV
(1)	857	611.5	77.8	79.9	421.6	32.2	58.5	59.3
(2)	358	306.9	75.2	36.8	194.9	0	58.3	58.6
(3)	50	55.1	23.6	31.2	0.3	0	54.0	52.9
(4)	37	40.1	15.2	24.7	0.2	0	51.7	50.8
(5)	15	20.1	6.9	13.2	< 0.07	0	41.8	40.8
(6-A)	0	0.41 ± 0.03	< 0.01	0.41	< 0.07	0	22.9	–
(6-B)	0	0.18 ± 0.02	0.02	0.16	< 0.07	0	–	18.9

Table 3: *The numbers of events after each cut for the data and the expected background for the tau channels. The background estimate is normalized to 10.4* pb^{-1}. *The quoted errors are statistical. The last two columns show the selection efficiencies, for cases A and B, for a 68* GeV *Higgs boson.*

6   The Electron and Muon Channels

The $\ell^+\ell^-q\bar{q}$ ($\ell = $ e or μ) final states arise mainly from the process $e^+e^-\rightarrow Z^0H^0\rightarrow\ell^+\ell^-q\bar{q}$. They amount to approximately 6% of the Higgs boson signal topologies with a small contribution (0.1% for m_{H^0}=68 GeV) from the Z^0Z^0 fusion process $e^+e^-\rightarrow e^+e^-H^0\rightarrow e^+e^-q\bar{q}$.

The analysis adopted concentrates on those final states proceeding through the first process. These yield a clean experimental signature in the form of large visible energy, two energetic, isolated, oppositely-charged leptons of the same species reconstructing to the Z^0 boson mass, and two energetic hadronic jets. The dominant backgrounds are $Z^0/\gamma^*\rightarrow q\bar{q}$ and four-fermion processes.

The selection proceeds as follows:

(1) The selected events are required to have at least six tracks and are reconstructed as four jets, using the Durham algorithm with a cut of $y_{34} > 0.001$ (single electrons or

muons are considered as low-multiplicity "jets"). The events must satisfy the relations $|p^z_{\mathrm{vis}}| < (E_{\mathrm{vis}} - 0.5\sqrt{s})$ and $E_{\mathrm{vis}} > 0.6\sqrt{s}$.

(2) The selected events must contain at least one pair of oppositely charged, same flavor leptons (e or μ). Muon candidates are identified using standard algorithms [27]. The identification of electron candidates, optimized for high energy electrons, starts by selecting electromagnetic calorimeter clusters having energy larger than 5 GeV and 90% of the cluster energy is deposited in four or five calorimeter cells at most, if the polar angle of the cluster satisfies $|\cos\theta| < 0.75$ or $|\cos\theta| > 0.75$, respectively. If such a cluster is found, tracks are sought within 5.7° of the cluster, having a momentum larger than 2 GeV and normalized energy-to-momentum ratios [5], $(E/p)_{\mathrm{norm}} > -5$. If more than one track satisfies these conditions, the one forming the smallest angle with the cluster direction is considered as the electron track. In the region $|\cos\theta| < 0.85$, other clusters within 10° of the original one are merged, provided that there is no other track within 20° .

Muon candidates are grouped into pairs without further restrictions. For an electron pair to be considered, at least one electron candidate must have $-2.5 < (E/p)_{\mathrm{norm}} < 5$.

If more than one pair of leptons of the same flavor is found, the pair with invariant mass closest to the Z^0 boson mass is considered.

(3) Both leptons in the candidate pair must have an energy larger than 20 GeV with at least one of them larger than 30 GeV. The energy of an electron candidate is obtained from the associated electromagnetic clusters while for a muon candidate it is approximated by the track momentum.

(4) The rest of the event, obtained by excluding the candidate lepton pair, is reconstructed as two jets using the Durham algorithm. An explicit lepton isolation cut is made to reject the remaining background from $Z^0/\gamma^* \to q\bar{q}(\gamma)$ with real or fake leptons close to the hadronic jets, by requiring that each of the leptons has a transverse momentum, calculated with respect to the nearest jet axis, larger than 10 GeV. The background from $e^+e^- \to Z^0/\gamma^* + Z^0/\gamma^*$ is suppressed by requiring that the opening angle of the jet pair be larger than 50°.

(5) The selected events must have a lepton pair with an invariant mass consistent with the Z^0 boson mass. For electrons the invariant mass of the lepton pair must lie between 75 GeV and 105 GeV, while for muons it must lie between 60 GeV and 120 GeV. The differing mass windows take into account the differing resolutions for electrons and muons.

Distributions of the lepton energy and of the lepton pair invariant mass are shown in Figures 9 and 10, for the data, the simulated background, and for a simulated signal having m_{H^0}=68 GeV. The numbers of observed and expected events after each stage of the selection are given in Table 4, together with the detection efficiency for a 68 GeV Higgs boson. After all cuts, no event survives in either the electron and muon channels, while in total $0.14 \pm 0.02(\mathrm{stat}) \pm 0.06(\mathrm{syst})$ events are expected.

---

[5] $(E/p)_{\mathrm{norm}} = [(E/p)-1]/\sigma$ where E and p are cluster energies and track momenta, and σ the error associated to E/p, obtained from the measurement errors of E and p.

The detection efficiencies as a function of the Higgs boson mass are given in Table 5. These are affected by the following systematic uncertainties: Monte Carlo statistics, 1.0% (electron), 0.9% (muon); uncertainties in the electron (muon) identification, 0.5% (0.4%); uncertainties in the modeling of fragmentation and hadronization, 0.3%; uncertainties in modeling the cut variables excluding lepton identification, 0.4%. Taking these uncertainties as independent and adding them in quadrature results in a total systematic uncertainty of 1.2% for the electron channel and 1.1% for the muon channel (relative errors).

Cut	Data	Total bkg.	$q\bar{q}(\gamma)$	4-ferm.	Efficiency m_{H^0}=68 GeV	
					electron (%)	muon (%)
(1)	313	335.9	246.1	89.8	88.9	82.8
(2)	71	75.1	52.7	22.4	75.1	78.0
(3)	2	2.0	0.9	1.1	70.5	74.9
(4)	1	0.7	0.2	0.6	67.9	72.1
(5)	0	0.14±0.02	0.02	0.12	65.3	70.3

Table 4: *The numbers of events after each cut for the data and the expected background in the lepton channels. Background estimates are normalized to the integrated luminosity. The quoted error is statistical. The last two columns show the detection efficiencies for the processes* $e^+e^- \rightarrow (e^+e^-$ *or* $\mu^+\mu^-$*)* H^0 *for a 68* GeV *Higgs boson.*

7 Mass Limit for the Standard Model Higgs boson

The signal detection efficiencies and the numbers of expected signal events, as a function of the Higgs boson mass, are summarized for all search channels in Table 5.

The following uncertainties affecting the numbers of expected signal events are common to all search channels: the uncertainty in the integrated luminosity: 0.6%; the uncertainty in the Higgs boson production cross section [13], which includes that from the collider energy: 1%; and the uncertainty in the Higgs decay branching ratios: 2% [5, 13]. Taking these uncertainties as independent and adding them in quadrature results in a systematic error, common to all search channels, of 3% (relative). In estimating the number of expected events for an assumed Higgs boson mass, these uncertainties are added in quadrature to those affecting the individual search channels.

To derive a new limit on the Higgs boson mass, this search, with one candidate event in the four jets channel at 172 GeV (m_{H^0}=75.6 ± 3.0 GeV where the error is on a Gaussian fit to the peak of a 75GeV Higgs MC distribution) is combined with earlier OPAL searches at $\sqrt{s} \approx m_{Z^0}$ with one candidate in the leptonic channel (m_{H^0}=61.2 ± 1.0 GeV) and 161 GeV [4], with one candidate in the missing energy channel (m_{H^0}=39.3±4.9 GeV). Two candidates from earlier searches with m_{H^0}< 25 GeV are not considered further. The expected numbers of Higgs

boson events, from this search and the combination of the present and earlier OPAL searches, are listed in the last two columns of Table 5. These numbers are affected by total uncertainties of less than 10%.

m_{H^0} (GeV)	$q\bar{q}H^0$ $H^0\to b\bar{b}$	$\nu\bar{\nu}H^0$	$\tau^+\tau^-H^0$ $H^0\to q\bar{q}$	$q\bar{q}H^0$ $H^0\to\tau^+\tau^-$	$e^+e^-H^0$	$\mu^+\mu^-H^0$	$\sqrt{s}$ =170-172 GeV	Grand total
40.0	14.6(1.7)	34.0(1.4)	28.3(0.2)	2.4(0.0)	59.6(0.4)	67.0(0.4)	4.1	106.1
50.0	21.7(2.1)	42.0(1.4)	28.7(0.1)	8.3(0.1)	63.0(0.3)	71.0(0.4)	4.4	34.8
55.0	24.7(2.1)	46.6(1.3)	28.0(0.1)	11.6(0.1)	63.2(0.3)	70.1(0.3)	4.3	19.6
60.0	27.0(1.9)	46.9(1.2)	26.6(0.1)	15.1(0.1)	63.6(0.3)	69.4(0.3)	3.8	12.1
65.0	28.2(1.7)	44.4(0.9)	24.5(0.1)	17.9(0.1)	64.8(0.2)	69.7(0.2)	3.2	6.7
67.5	28.4(1.5)	43.0(0.8)	23.2(0.1)	18.8(0.1)	65.2(0.2)	70.2(0.2)	2.8	4.7
68.0	28.4(1.5)	42.7(0.8)	22.9(0.1)	18.9(0.1)	65.3(0.2)	70.3(0.2)	2.8	4.4
70.0	28.2(1.3)	41.3(0.7)	21.7(0.1)	19.3(0.1)	65.3(0.2)	70.6(0.2)	2.4	3.2
75.0	26.6(0.8)	34.3(0.4)	18.2(0.0)	18.3(0.0)	63.5(0.1)	71.3(0.1)	1.5	1.6
80.0	23.3(0.2)	19.2(0.1)	14.0(0.0)	14.1(0.0)	57.6(0.0)	70.8(0.0)	0.4	0.4

Table 5: *Detection efficiencies (in %) and numbers of expected Higgs boson events (between parentheses) at 172 GeV for each search channel separately as a function of the Higgs boson mass. The quoted efficiencies are obtained from a fit to values determined at fixed values of m_{H^0}. The last two columns show the total numbers of expected events in the present search at 170 and 172 GeV, and the grand total, which also includes the expectations from earlier OPAL searches at center-of-mass energies close to the Z^0 mass and the revised 161 GeV analysis.*

Figure 11 shows separately the number of expected events for the present search, for previous OPAL searches at the Z^0 peak and $\sqrt{s} = 161$ GeV [4] (where the revised 161 GeV analysis is implemented), and for their sum, as a function of the Higgs boson mass. Also shown is the 95% confidence level upper limit on the number of observed candidate events. A lower limit on the Higgs boson mass, of 69.4 GeV, is extracted at the 95% Confidence Level. In deriving this limit, the probability that a candidate event with a given observed mass actually originates from a Higgs boson of arbitrary mass is calculated following Ref. [29] which takes into account the experimental mass resolution including tails in the various search channels. The expected background is reduced by the systematic error per channel and then subtracted. It was found that the errors on the background estimation have marginal effects on the results, reducing the derived limit by 0.1 GeV. The systematic errors are incorporated into the limit according to the method prescribed in Ref. [30], reducing the derived limit by an additional 0.1 GeV. The effect of channels weighting and background subtraction is small. If all channels were assigned equal weights, irrespective of the expected rate and background, and no background subtraction had performed, the limit would have gone down to only 69.0 GeV.

Figure 12 shows the measured confidence level and the expected one (averaged over a large number of hypothetical experiments with no signal and candidates spread according to the expected background distributions) as a function of the Higgs boson mass. From this Figure it

can be seen that the expected limit is at 65.4 GeV and the expected C.L. for the experimental limit of 69.4 GeV is 82%. According to MC trial experiments a reasonable value of 11.8% was found for the probability of inferring a mass limit greater than or equal to 69.4 GeV assuming no contribution from a Higgs boson signal.

8 Summary

A new search is presented for the Standard Model Higgs boson produced in association with a fermion-antifermion pair. The search is based on data collected in 1996 by the OPAL experiment at center-of-mass energies of 170 and 172 GeV, with an integrated luminosity of 10.4 pb^{-1}. The data show no significant excess beyond the background predicted by the Standard Model. Combined with earlier OPAL searches at center-of-mass energies in the vicinity of the Z^0 resonance and a revised analysis of the 161 GeV data, this search leads to a lower limit of 69.4 GeV for the mass of the Standard Model Higgs boson, at the 95% confidence level.

References

[1] S. L. Glashow, J. Iliopoulos and L. Maiani, Phys. Rev. **D2** (1970) 1285;
   S. Weinberg, Phys. Rev. Lett. **19** (1967) 1264;
   A. Salam, *Elementary Particle Theory*, ed. N. Svartholm (Almquist and Wiksells, Stockholm, 1968), 367.

[2] P. W. Higgs, Phys. Lett. **12** (1964) 132;
   F. Englert and R. Brout, Phys. Rev. Lett. **13** (1964) 321;
   G. S. Guralnik, C. R. Hagen, and T. W. B. Kibble, Phys. Rev. Lett. **13** (1964) 585.

[3] ALEPH Collaboration, D. Buskulic *et al.*, Phys. Lett. **B384** (1996) 427;
   DELPHI Collaboration, P. Abreu *et al.*, Nucl. Phys. **B421** (1994) 3;
   L3 Collaboration, M. Acciarri *et al.*, Phys. Lett. **B385** (1996) 454;
   OPAL Collaboration, G. Alexander *et al.*, Z. Phys. **C73** (1997) 189.

[4] OPAL Collaboration, K. Ackerstaff *et al.*, CERN-PPE/96-161, Phys. Lett. **B393** (1997) 231.

[5] A. Djouadi, M. Spira, and P. M. Zerwas, Z. Phys. **C70** (1996) 425.

[6] OPAL Collaboration, K. Ahmet *et al.*, Nucl. Inst. and Meth. **A305** (1991) 275.

[7] P. P. Allport *et al.*, Nucl. Inst. and Meth. **A346** (1994) 476;
   S. Anderson *et al.*, submitted to Nucl. Inst. and Meth. **A**.

[8] B.E. Anderson *et al.*, IEEE Transactions on Nuclear Science **41** (1994) 845.

[9] OPAL Collaboration, K. Ackerstaff *et al.*, Phys. Lett. **B391** (1997) 221.

[10] OPAL Collaboration, R. Akers *et al.*, Phys. Lett. **B327** (1994) 397.

[11] J. Allison *et al.*, Nucl. Inst. and Meth. **A317** (1992) 47.

[12] HZHA generator: P. Janot, in *Physics at LEP2*, edited by G. Altarelli, T. Sjöstrand and F. Zwirner, CERN 96-01, vol. 2 (1996), p. 309. For Higgs production cross sections see also [13].

[13] E. Gross, B. A. Kniehl, and G. Wolf, Z. Phys. **C63** (1994) 417; erratum *ibid.* **C66** (1995) 32.

[14] PYTHIA 5.721 and JETSET 7.408 generators: T. Sjöstrand, Comp. Phys. Comm. **82** (1994) 74; T. Sjöstrand, LU TP 95-20.

[15] The grc4f 1.1 generator: J. Fujimoto *et al.*, Comput. Phys. Commun. 100 (1997) 128. J. Fujimoto *et al.*, in *Physics at LEP2*, edited by G. Altarelli, T. Sjöstrand and F. Zwirner, CERN 96-01, vol. 2 (1996) p. 30.

[16] BHWIDE generator: S. Jadach, W. Płaczek, B.F.L. Ward, in *Physics at LEP2*, edited by G. Altarelli, T. Sjöstrand and F. Zwirner, CERN 96-01, vol. 2 (1996), p. 286; UTHEP-95-1001.

[17] KORALZ 4.0 generator: S. Jadach, B. F. L. Ward, Z. Wąs, Comp. Phys. Comm. **79** (1994) 503.

[18] PHOJET 1.05 generator: E. Budinov *et al.*, in *Physics at LEP2*, edited by G. Altarelli, T. Sjöstrand and F. Zwirner, CERN 96-01, vol. 2 (1996) p. 216; R. Engel and J. Ranft, Phys. Rev. **D54** (1996) 4244.

[19] J.A.M. Vermaseren, Nucl. Phys. **B229** (1983) 347.

[20] OPAL Collaboration, G. Alexander *et al.*, Z. Phys. **C52** (1991) 175.

[21] OPAL Collaboration, G. Alexander *et al.*, Phys. Lett. **B376** (1996) 232.

[22] N. Brown and W. J. Stirling, Phys. Lett. **B252** (1990) 657; S. Bethke, Z. Kunszt, D. Soper and W. J. Stirling, Nucl. Phys. **B370** (1992) 310; S. Catani *et al.*, Phys. Lett. **B269** (1991) 432; N. Brown and W. J. Stirling, Z. Phys. **C53** (1992) 629.

[23] G. Parisi, Phys. Lett. **B74** (1978) 65; J. F. Donoghue, F. E. Low and S. Y. Pi, Phys. Rev. **D20** (1979) 2759.

[24] OPAL Collaboration, R. Akers *et al.*, Z. Phys. **C65** (1995) 17.

[25] OPAL Collaboration, R. Akers *et al.*, Phys. Lett. **B327** (1994) 411.

[26] OPAL Collaboration, G. Alexander *et al.*, Z. Phys. **C70** (1996) 357.

[27] OPAL Collaboration, G. Alexander *et al.*, Z. Phys. **C52** (1991) 175.

[28] OPAL Collaboration, R. Akers *et al.*, Z. Phys **C63** (1994) 197.

[29] P. Bock, *Determination of exclusion limits for particle production using different decay channels with different efficiencies, mass resolutions and backgrounds*, Heidelberg University preprint HD-PY-96/05 (1996).

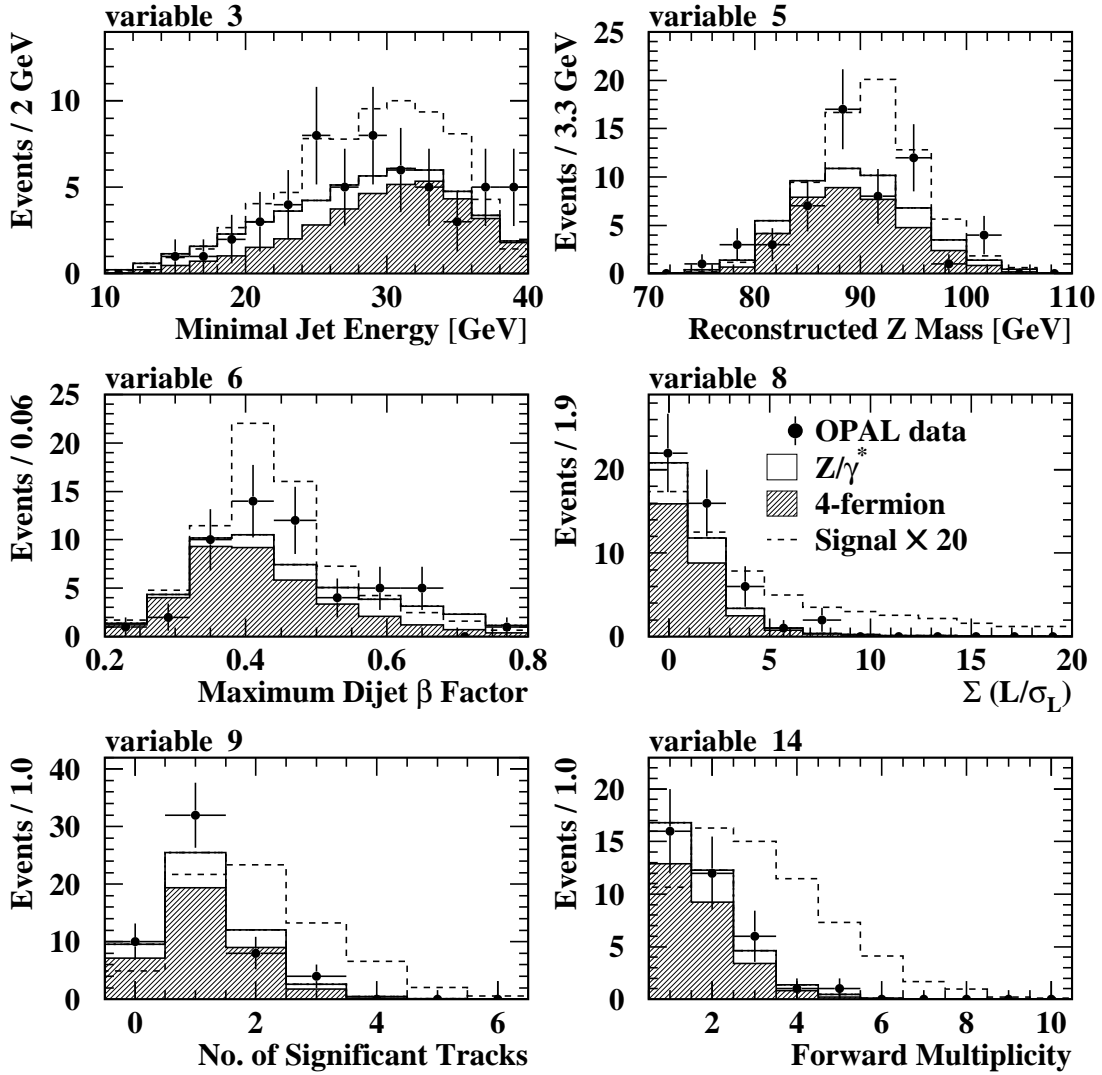[30] R. D. Cousins, V. L. Highland, Nucl. Inst. and Meth. **A320** (1992) 331.

OPAL

Figure 1: Four jets channel: distribution of input variables 3,5,6,8,9 and 14 (as described in the text) for OPAL data at $\sqrt{s}$=170 and 172 GeV compared with the Monte Carlo expectations; data: points with error bars, simulations (normalized to recorded luminosity): open / shaded / dashed histograms for $Z^0/\gamma^* \to q\bar{q}$ / four-fermion processes / signal (m_{H^0}=68 GeV) scaled by a factor of 20. All distributions are shown after the preselection (cuts 1-6).
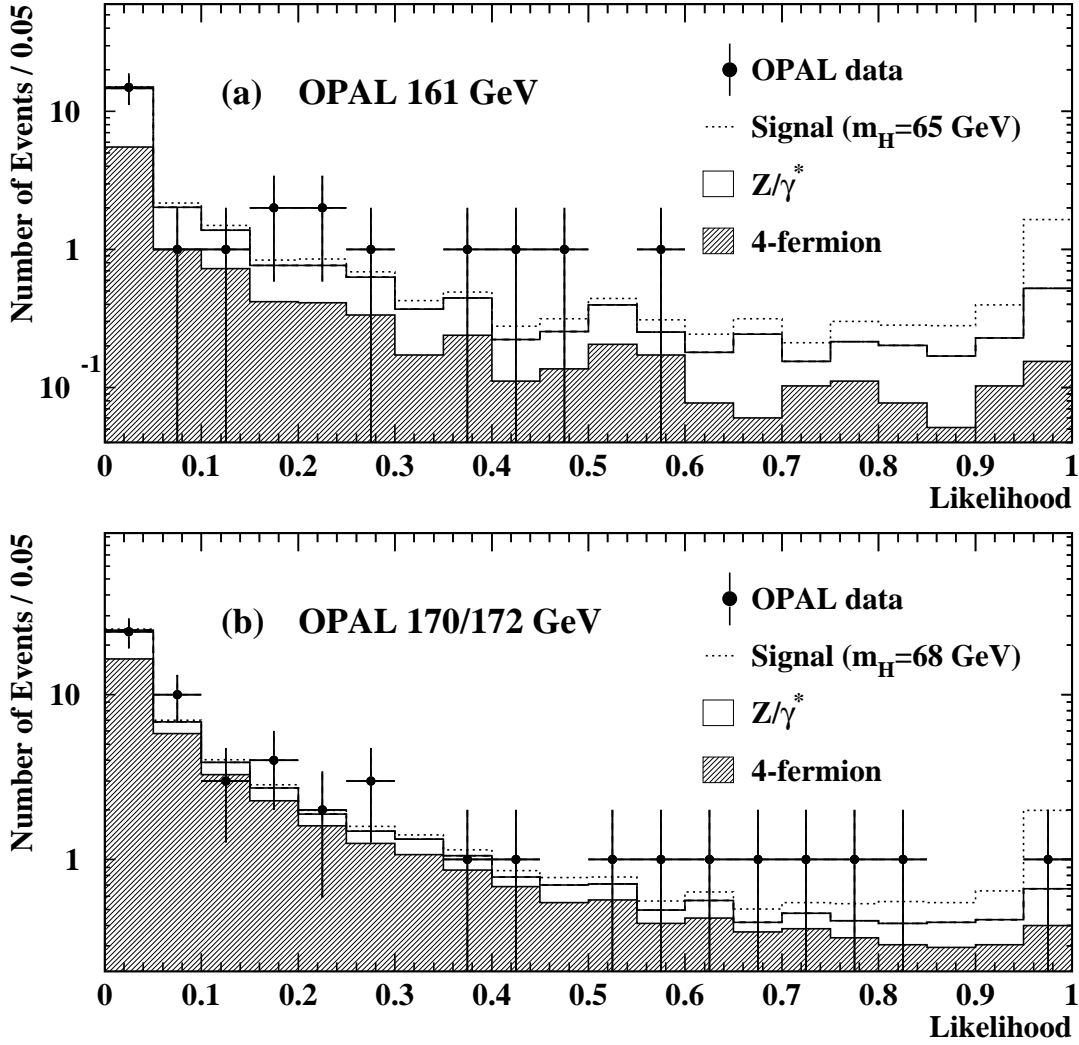
Figure 2: Four jets channel: (a) Likelihood distribution for OPAL data at $\sqrt{s} = 161$ GeV compared with the Monte Carlo expectation. (b) Likelihood distribution for OPAL data at $\sqrt{s} = 170$ and 172 GeV compared with the Monte Carlo expectation. All distributions are shown after the preselection (cuts 1-6).
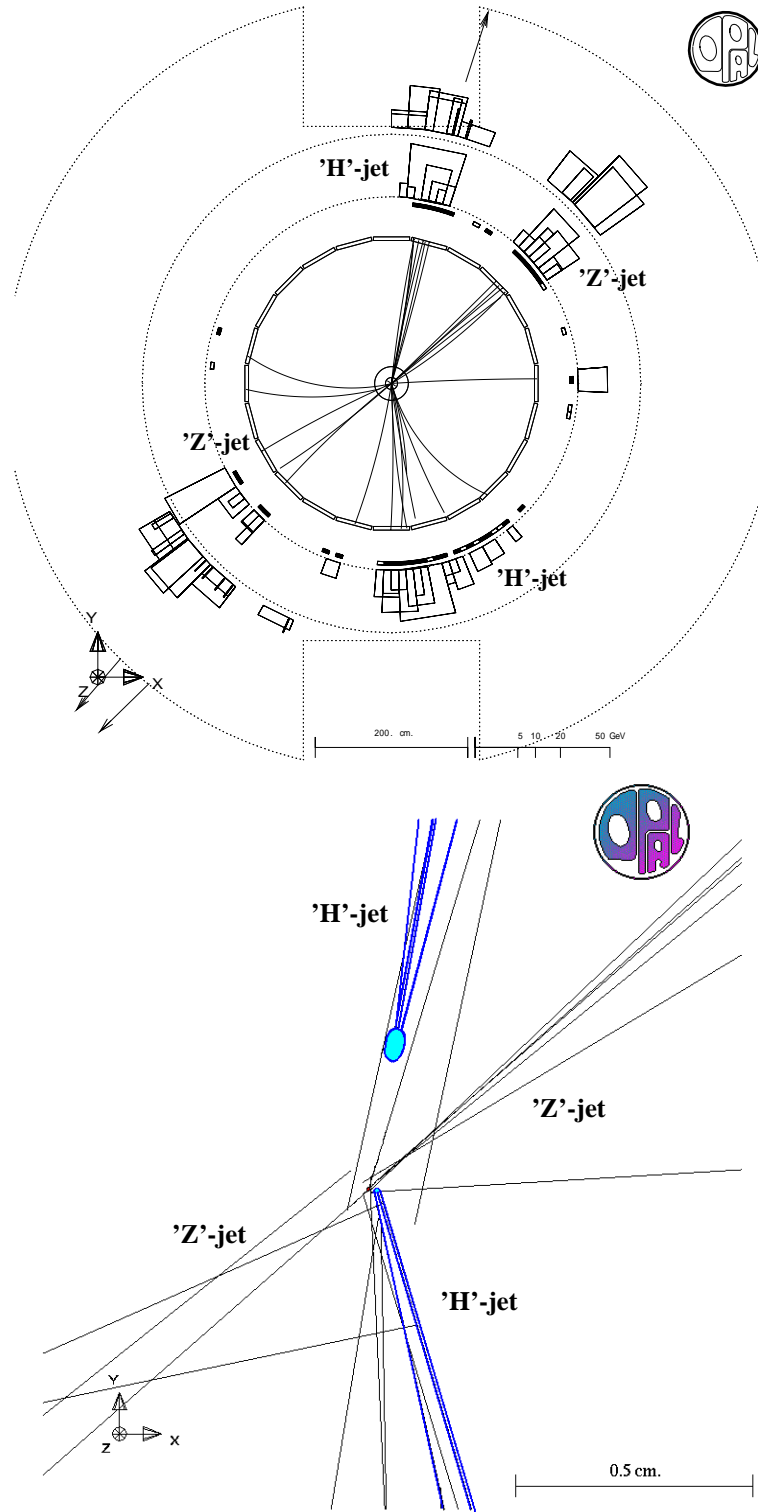
Figure 3: The candidate event in the four jet channel. Top: $r\phi$ view with tracks and clusters; bottom: zoom in on the vertex region. The jets associated to the Higgs in the kinematic fit yielding the highest probability, are labeled as Higgs jets ('H'-jet); the others are labeled as Z^0 jets ('Z'-jet). The error ellipse of the second Higgs jet is too small to be seen in this plot.
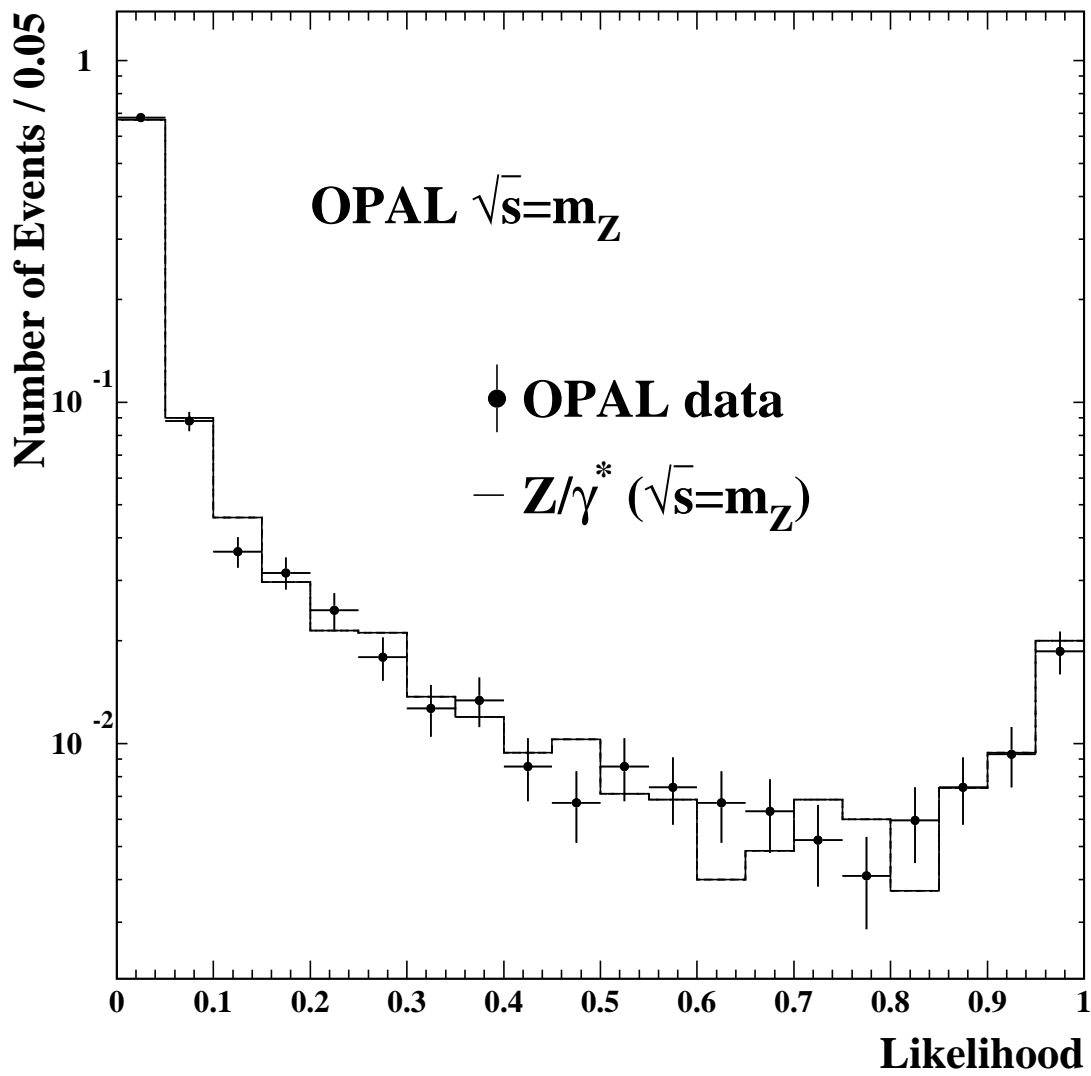
Figure 4: Four jets channel: likelihood distribution of OPAL events at $\sqrt{s} = m_{Z^0}$ scaled to LEP 2 energies compared with the Monte Carlo expectation.
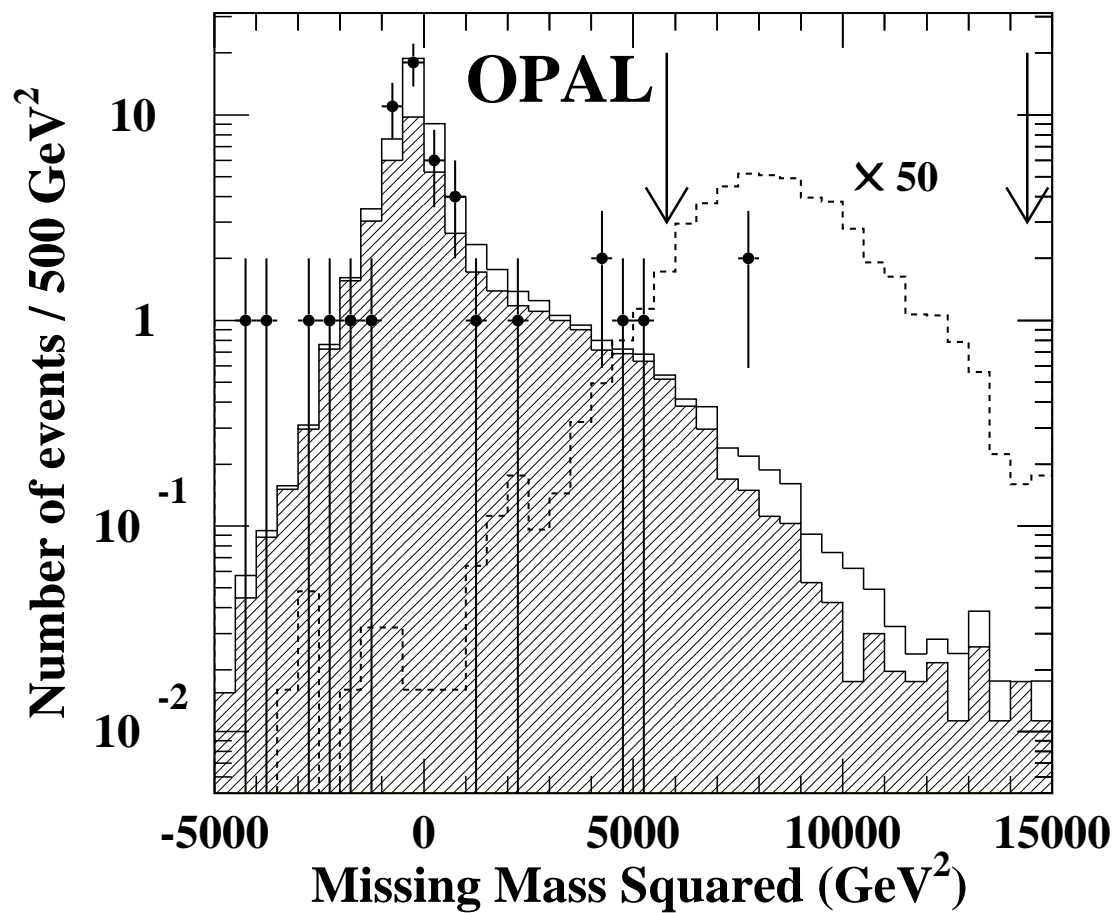
Figure 5: Missing energy channel; distributions of the missing mass squared after cut (5) data: points with error bars, simulations (normalized to recorded luminosity): open / shaded / dashed histograms for $Z^0/\gamma^* \to q\bar{q}$ / four-fermion processes / signal (m_{H^0}=68 GeV) scaled by a factor of 50; The arrows indicate the cut position, $76^2 < m^2_{\text{miss}} < 120^2$ GeV^2.
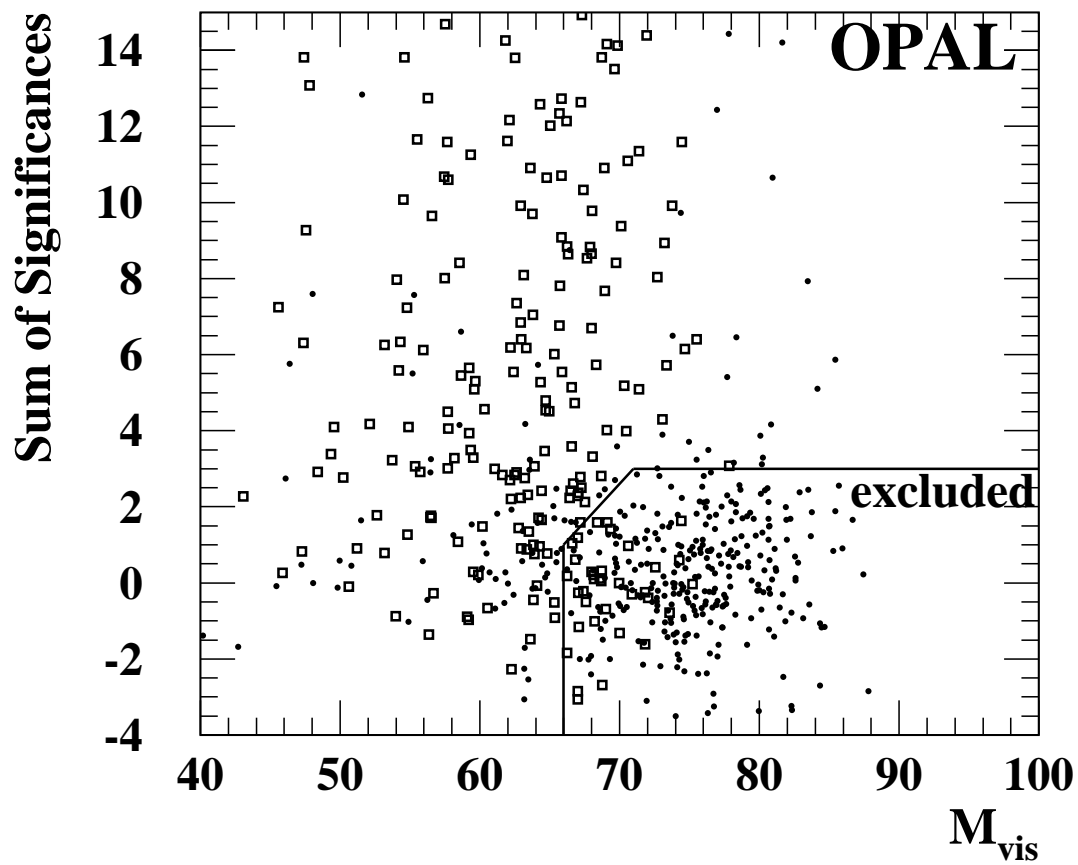
Figure 6: Missing energy channel; scatter plot of Σ_S vs. the visible mass, after cut (7); dots: simulated four-fermion background; open squares: signal for m_{H^0}=68 GeV. straight line: cut region. The one event (not shown) which survived the cuts, is at a visible mass of 67.7 GeV and Σ_S=1.6.
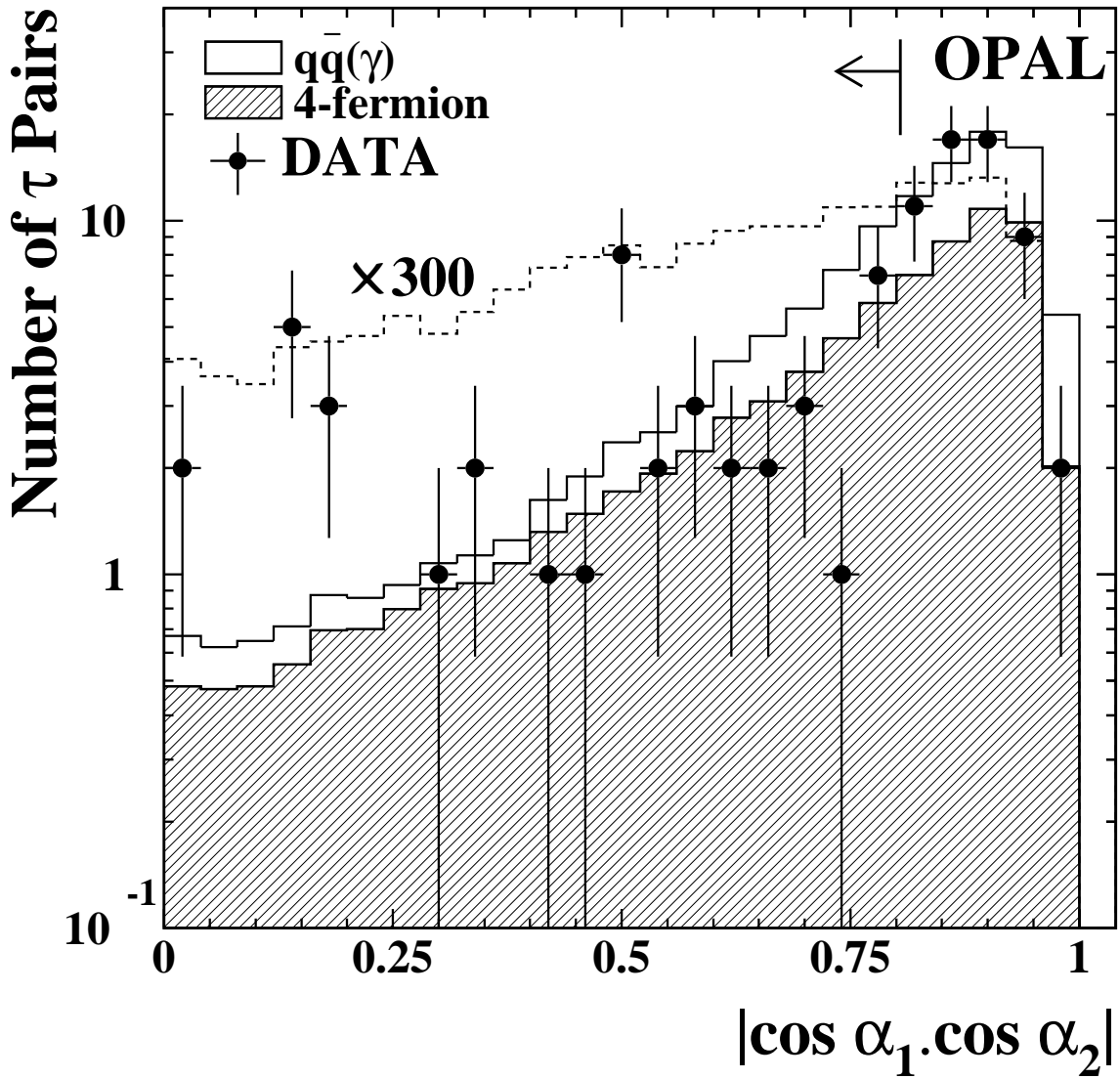
Figure 7: Tau channels; distributions of the pairwise isolation parameter (see text) after cut (3); data: points with error bars, simulations (normalized to recorded luminosity): open / shaded / dashed histograms for $Z^0/\gamma^* \rightarrow q\bar{q}$ / four-fermion processes / signal ($m_{H^0}=68$ GeV). Arrows indicate domains accepted by the cuts.
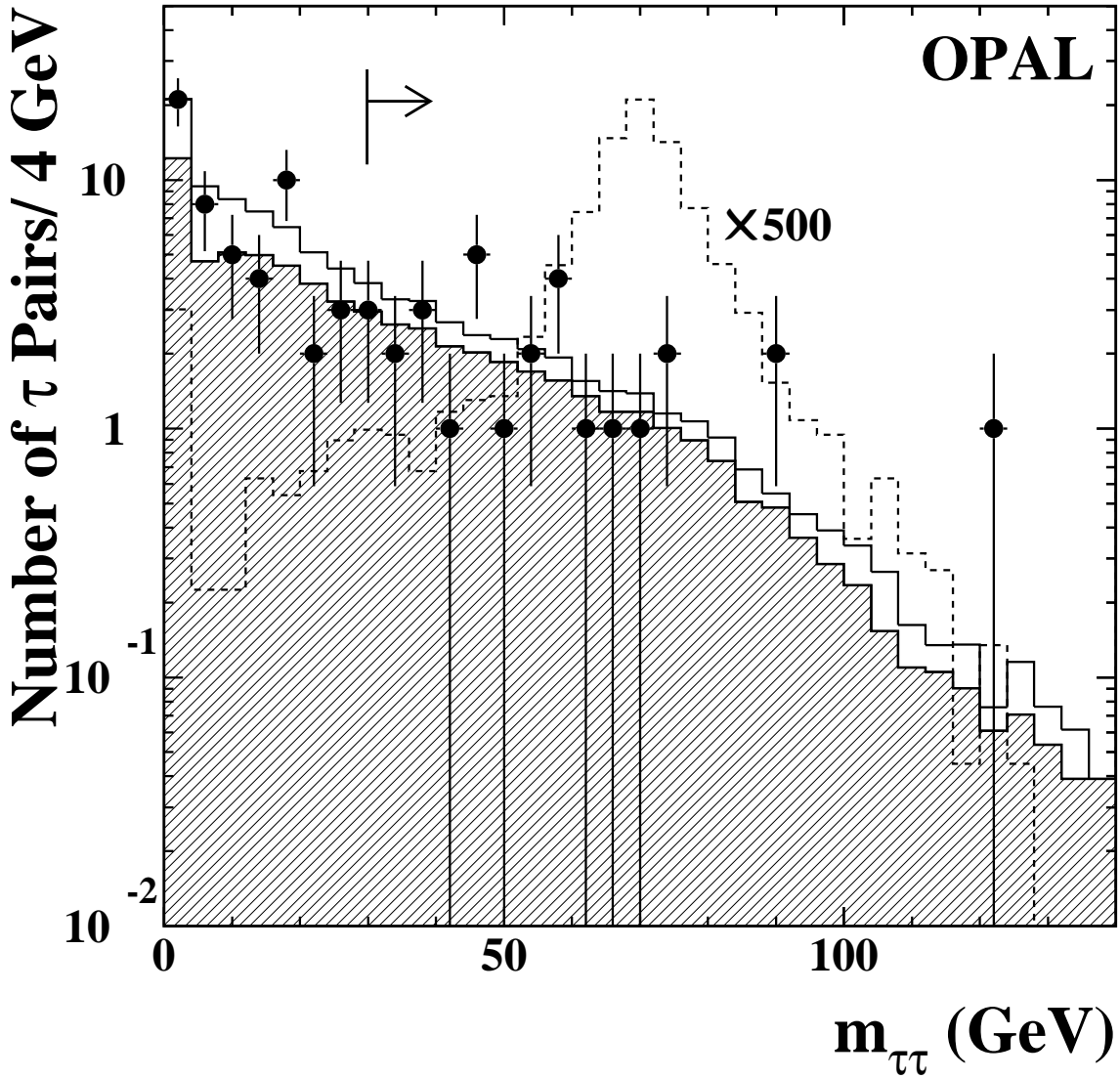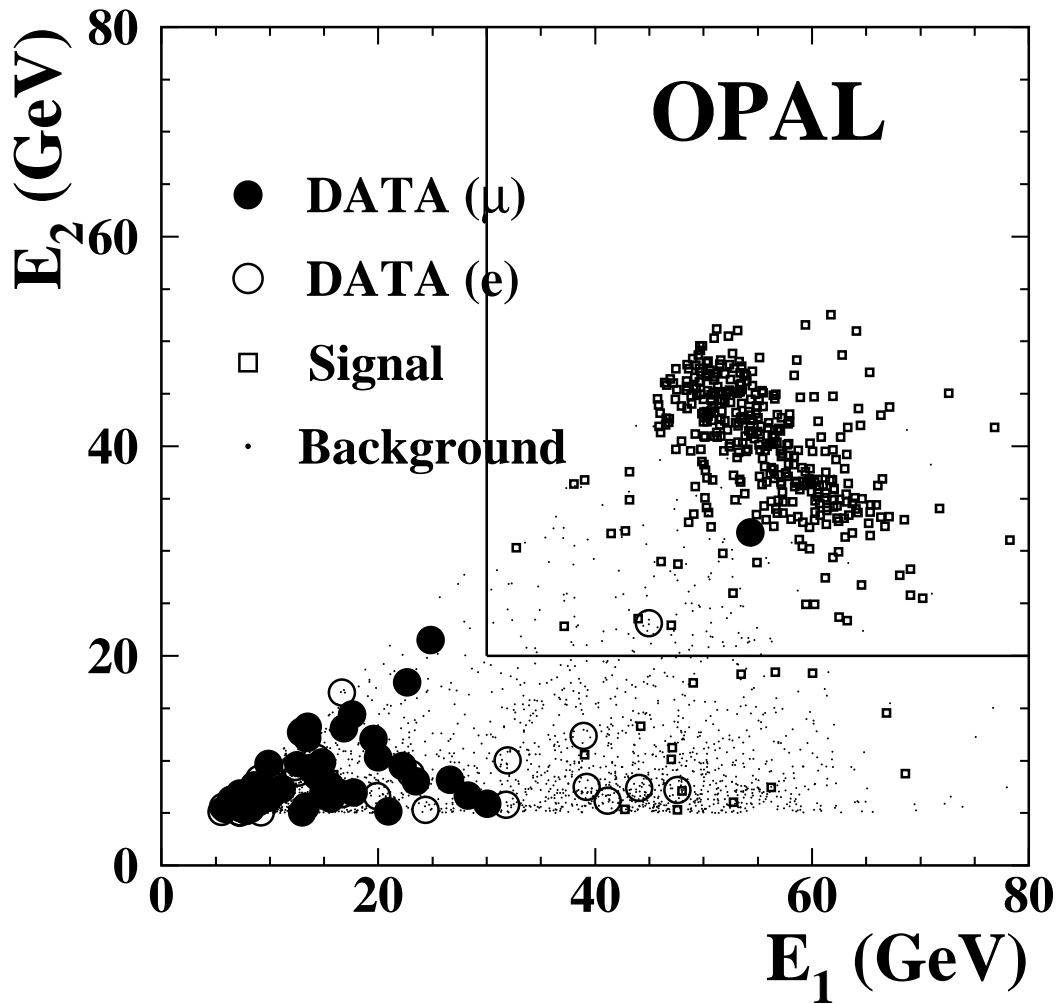
Figure 8: Tau channels; distributions of the $\tau^+\tau^-$ invariant mass after cut (4); data: points with error bars, simulations (normalized to recorded luminosity): open / shaded / dashed histograms for $Z^0/\gamma^* \to q\bar{q}$ / four-fermion processes / signal (m_{H^0}=68 GeV). Arrows indicate domains accepted by the cuts.

Figure 9: Electron and muon channels; scatter plot of the energies of the lepton candidates, after cut (2). The symbols for the data and the simulated signal (m_{H^0}=68 GeV, e^+e^- and $\mu^+\mu^-$ channels combined) as indicated; small dots: simulated backgrounds. Solid lines: position of cut (3).
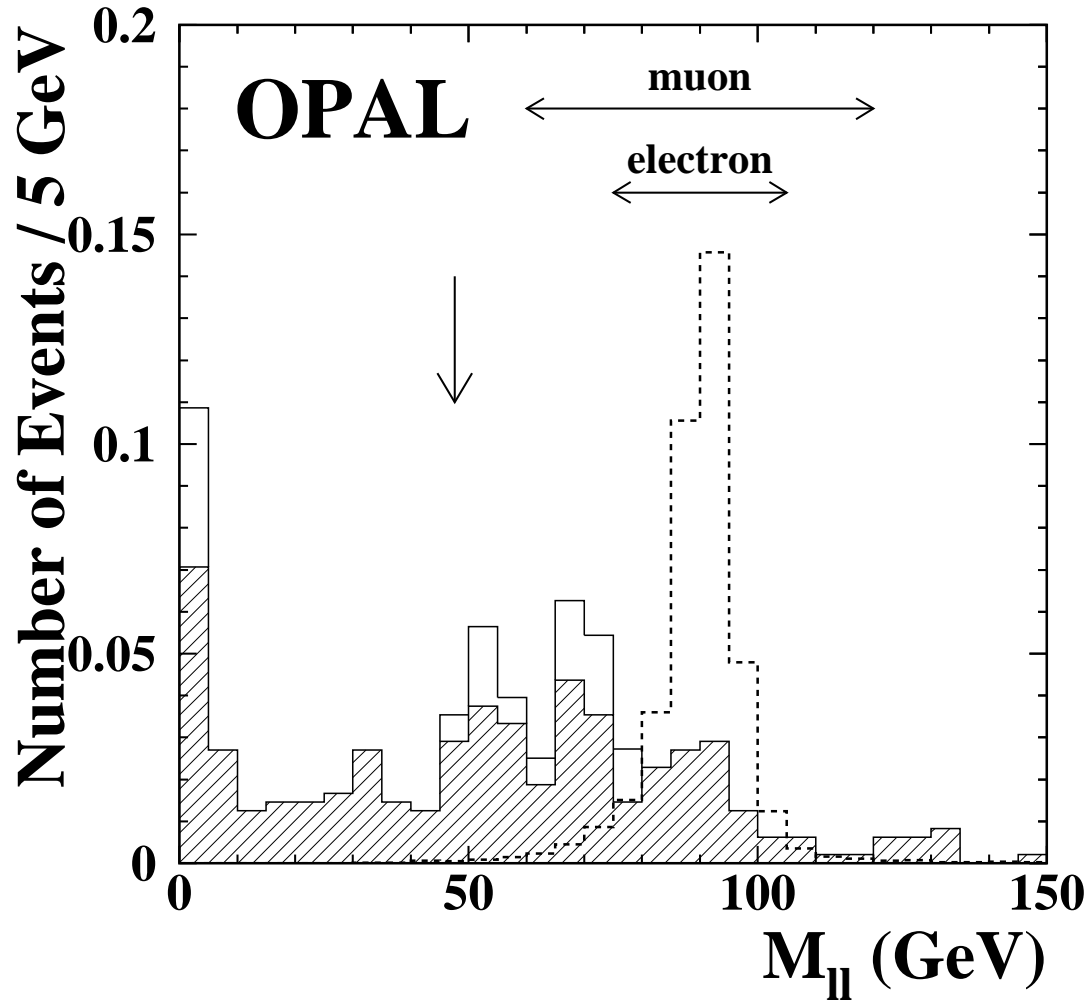
Figure 10: Electron and muon channels; invariant mass of the lepton pair, after cut (4). Open / shaded / dotted histograms: $Z^0/\gamma^* \to q\bar{q}$ / four-fermion backgrounds / simulated signal (m_{H^0}=68 GeV, e^+e^- and $\mu^+\mu^-$ channels combined). All simulations are normalized to the integrated luminosity. Horizontal arrows: selected mass ranges; vertical arrow: invariant mass of the event remaining in the e^+e^- channel after cut (4).
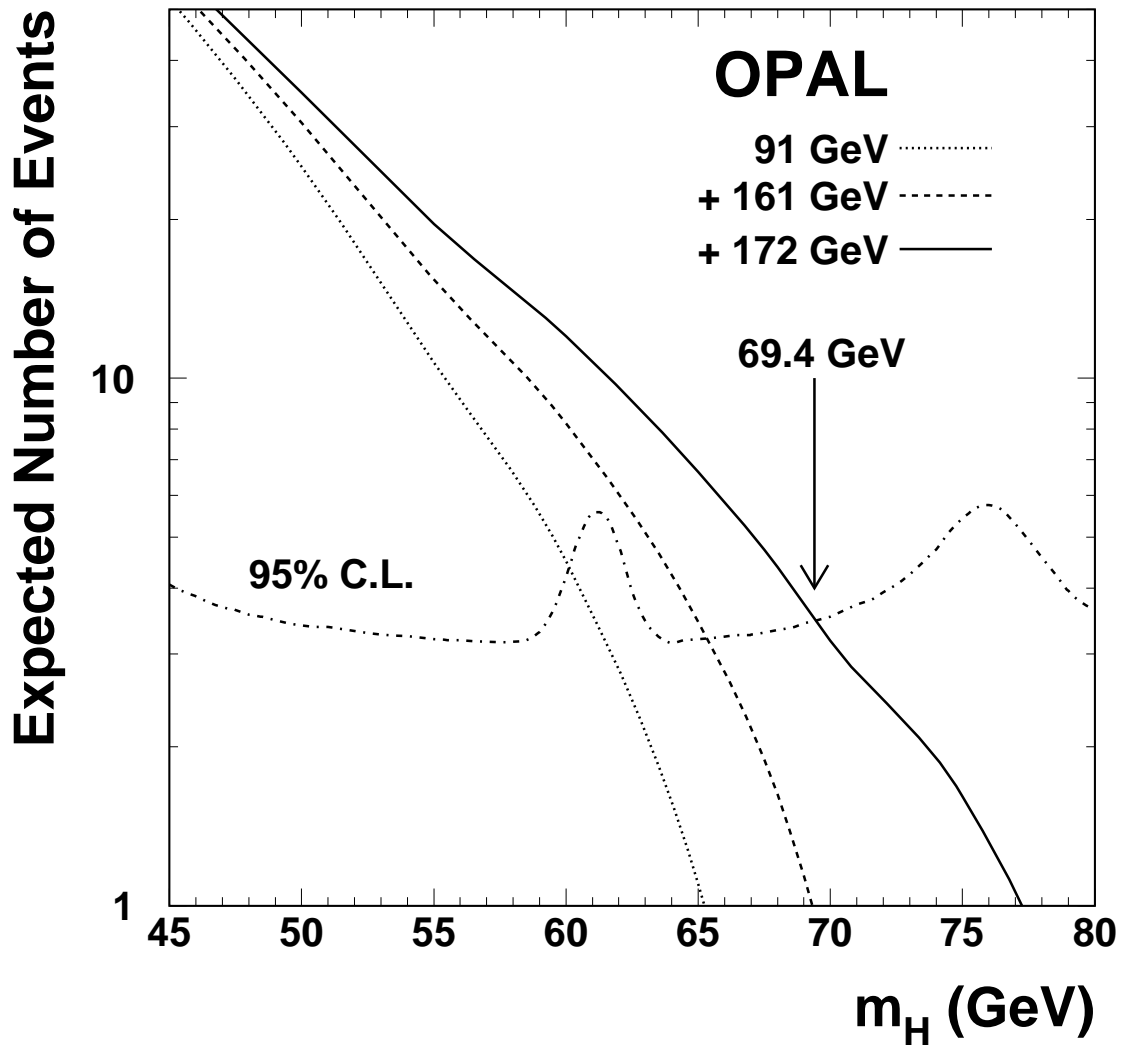
Figure 11: Expected number of events as a function of the Higgs boson mass. OPAL searches at $\sqrt{s}=m_{Z^0}$ (dotted), including $\sqrt{s}$=161 GeV (dashed) and the grand total (full line) including OPAL searches at $\sqrt{s}$=170/172 GeV. The dash-dotted horizontal line is the 95% confidence level upper limit for a possible Higgs boson signal in the presence of the observed high-mass candidate events (see text). The intersection of the solid curve with the dash-dotted curve, indicated by the arrow, determines the 95% confidence level lower limit obtained for the Higgs boson mass;
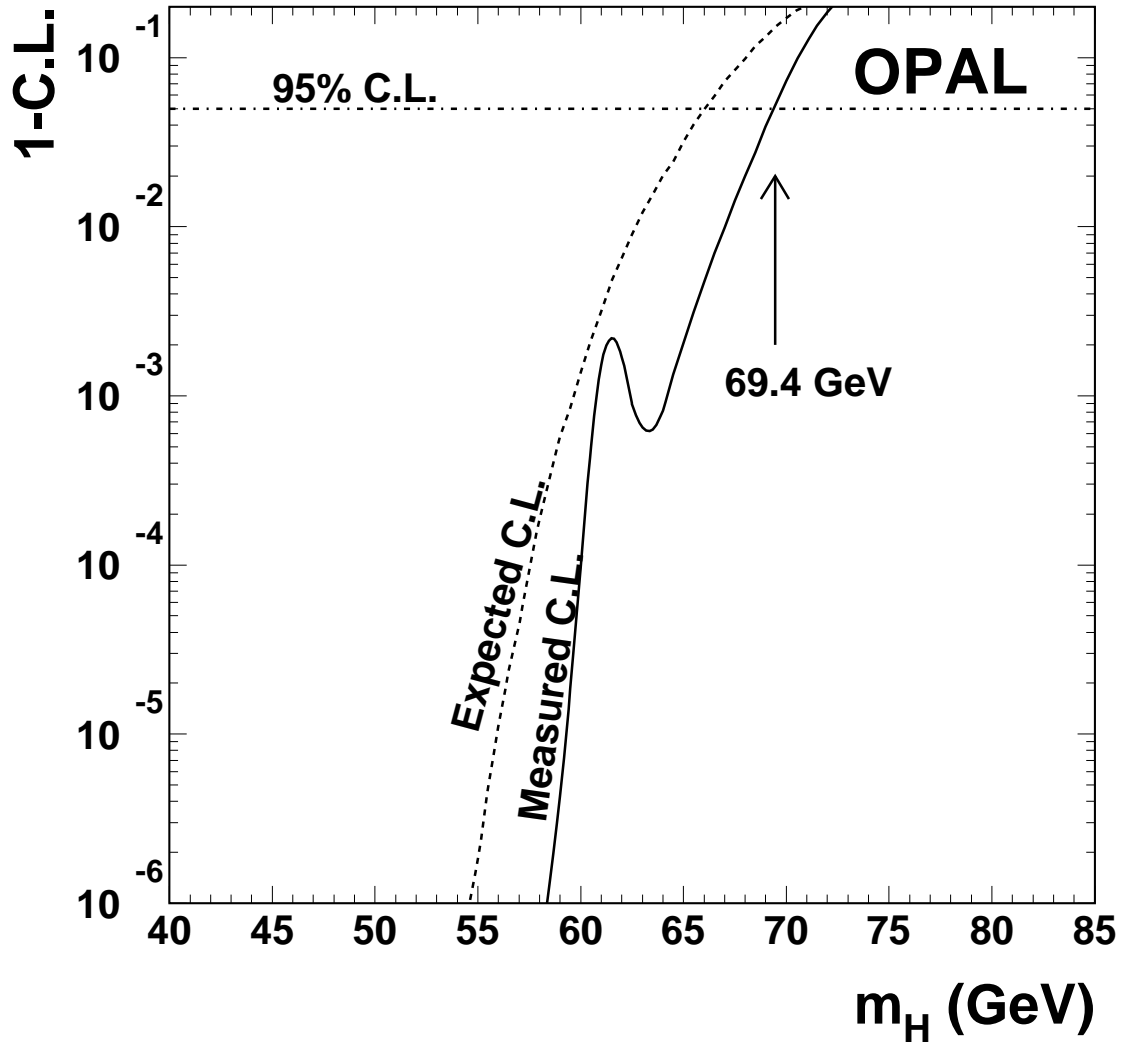
Figure 12: The expected (dashed) and measured (solid) Confidence Level (1-C.L.) as a function of the Higgs boson mass when all channels at all center-of-mass energies are combined. The intersection of the 95% C.L. line (dash-dotted) with the dashed and solid curves determines the 95% expected and measured (respectively) confidence level lower limits obtained for the Higgs boson mass; the latter is indicated by an arrow.